Tectonophysics, 211 (1992) 149–178
Elsevier Science Publishers B.V., Amsterdam

Earthquake source nucleation: a physical model for short-term precursors

Mitiyasu Ohnaka

Earthquake Research Institute, University of Tokyo, Bunkyo-ku, Tokyo 113, Japan

(Received March 18, 1991; revised version accepted January 10, 1992)

ABSTRACT

Ohnaka, M., 1992. Earthquake source nucleation: a physical model for short-term precursors. In: T. Mikumo, K. Aki, M. Ohnaka, L.J. Ruff and P.K.P. Spudich (Editors), Earthquake Source Physics and Earthquake Precursors. *Tectonophysics*, 211: 149–178.

This paper deals with a quasistatic, leading to a quasidynamic at a later time, nucleation process that precedes the earthquake dynamic rupture, and models of the earthquake source nucleation are put forward based on physical principles. A quasistatic to quasidynamic rupture nucleation process is an intrinsic part of the ensuing earthquake dynamic rupture; in other words, the nucleation process itself is an short-term (or immediate) precursor that occurs in a localized zone. During the earthquake nucleation, premonitory slip proceeds in the localized nucleation zone, and shear stress also decreases gradually in the zone, since slip-weakening occurs during the nucleation. Immediate foreshock activity is a part of the nucleation process leading to the mainshock dynamic rupture; therefore, hypocentral locations of foreshocks are necessarily restricted to lie near the mainshock hypocentre (onset of the mainshock rupture). Whether or not foreshocks occur during the mainshock nucleation depends on how the rupture growth resistance varies on a local to small scale. Since patches of greater rupture growth resistance are considered to prevail on a local to small scale in the fault zone, carrying immediate foreshocks would be one of the major characteristics of earthquakes that nucleate within the brittle seismogenic layer. When a mainshock earthquake nucleates within the brittle seismogenic layer and its hypocentre is located near the base of the seismogenic layer, immediate foreshocks for this mainshock are necessarily restricted to lie within a localized region shallower than hypocentral depth of the mainshock. By contrast, the nucleation process below the base of the seismogenic layer is aseismic in nature, so that carrying no conspicuous foreshocks would be a common characteristic of interplate earthquakes that nucleate below the base of the brittle seismogenic layer. The breakdown strength τ_p, the breakdown stress drop $\Delta\tau_b$ and the critical slip displacement D_c are indicative of the rupture growth resistance. To estimate depth variations of these parameters, the effects of the normal stress σ_n and temperature T on those parameters are examined using available data so far published. The combined effects of σ_n and T on τ_p in the brittle to semibrittle regime are found to be represented empirically by:

$$\tau_p(\sigma_n, T) = \tau_{p0}(\sigma_n)[1 - (\cosh(50/T) + 40\sinh(50/T))\exp(-2000/T)]$$

where $\tau_{p0}(\sigma_n) = 135.7 + 0.750\sigma_n$, and T is measured in °K and σ_n in MPa. It is found that D_c increases sharply with T, but is insensitive to σ_n above 300°C, while D_c depends on σ_n but is insensitive to T below 300°C. On the basis of these results, variations in τ_p, D_c and $\Delta\tau_b$ at mid-crustal depths are estimated for quartzo-feldspathic rocks for a given geothermal gradient.

1. Introduction

Seismicity observations made for decades have shown that immediate foreshocks are concentrated in the vicinity of the epicentre of the pending mainshock, though it is certain that some major earthquakes (e.g., the 1989 Loma Prieta earthquake; U.S. Geological Survey Staff, 1990) carried no obvious immediate foreshocks. Observations with good location capability (Hamada, 1987) further indicate that such foreshocks are restricted to lie within a localized region near but

Correspondence to: M. Ohnaka, Earthquake Research Institute, University of Tokyo, Bunkyo-ku, Tokyo 113, Japan.

shallower than hypocentre depths of the mainshocks located near the base of the seismogenic layer. However, these observations have not been explained reasonably in terms of a model based on physical principles. On the other hand, it has been established that the earthquake source in the brittle seismogenic layer is slip-failure mechanical instability that gives rise to dynamically propagating shear rupture along a plane or thin zone of weakness (referred to as a preexisting fault). Thus, imminent preseismic and coseismic source processes, including the above observations, in individual tectonic settings should be described comprehensively in terms of the constitutive relation that governs the breakdown processes during brittle shear rupture or slip-failure along a weak junction (or zone). Recent experimental and theoretical studies (Ohnaka and Kuwahara, 1990; Yamashita and Ohnaka, 1991) have shown that stable, quasistatic to quasidynamic nucleation is an intrinsic part of the ensuing unstable dynamic rupture propagation, and hence it is crucial for the short-term prediction to understand the preparatory process (or nucleation) that precedes earthquake dynamic instability, since the nucleation process itself can be regarded as an immediate earthquake precursor.

In this paper, we first put forward a model of earthquake rupture nucleation based on physical principles, which explains why and how short-term (or immediate) precursors are intrinsically related to the earthquake source nucleation that proceeds quasistatically to quasidynamically prior to the mainshock dynamic rupture, and how essential it is for carrying immediate foreshocks that the rupture growth resistance is distributed inhomogeneously on a local to small scale in the fault zone. We then estimate, on the basis of laboratory data available, how the peak shear resistance, the critical slip displacement and the breakdown stress drop, which are indicative of the rupture growth resistance, vary with depth, particularly at mid-crustal depths characterised by semibrittle deformation. Spatial distribution of such rupture growth resistance prescribes whether rupture grows stably and quasistatically, or unstably and dynamically (Yamashita and Ohnaka, 1991). Finally we discuss specifically in terms of

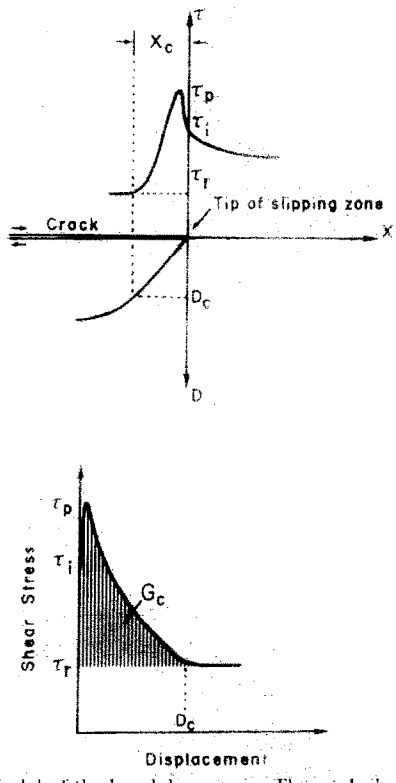

Fig. 1. A model of the breakdown zone. The peak shear stress τ_p is attained at a nonzero value of slip displacement; τ_i is the shear stress on the verge of slip at a crack-tip; τ_f is the residual frictional stress; D_c is the critical slip displacement, which is the slip displacement required for the shear stress to decrease to τ_f; X_c is the breakdown zone size; and G_c is the critical energy release rate. The breakdown stress drop $\Delta\tau_b$ is defined as the difference between τ_p and τ_f.

the proposed model the nucleation process of earthquakes for the two different cases: interplate earthquakes that nucleate below the base of the brittle seismogenic layer, and intraplate earthquakes that nucleate within the brittle seismogenic layer. It will be shown that immediate foreshock activity is a part of the mainshock earthquake nucleation.

2. Modelling of earthquake source nucleation

The breakdown process near the rupture front during slip failure is modelled as shown in Figure 1. This specific model has been justified by an increasing number of experimental and theoretical grounds (Ohnaka et al., 1986, 1987; Ohnaka and Yamashita, 1989; Ohnaka and Kuwahara,

1990; Ohnaka, 1990; Yamashita and Ohnaka, 1991; Matsu'ura et al., 1992). The model, often referred to as the breakdown zone model, is based on the slip-dependent constitutive relation, and is virtually characterized by the following three parameters: the peak shear stress (or the breakdown strength) τ_p, the breakdown stress drop (or the effective breakdown stress) $\Delta\tau_b$, and the critical slip displacement D_c. $\Delta\tau_b$ is defined as the difference between τ_p and a residual friction stress level τ_r, and D_c is defined as the slip displacement required for the local shear stress near a crack-tip to decrease to τ_r. The energy required for rupture growth is related to $\Delta\tau_b$ and D_c, and hence the parameters $\Delta\tau_b$ and D_c may be considered indicative of the rupture growth resistance. Slip-weakening begins to occur just after the shear stress at the crack-tip has reached the peak value τ_p, and in this sense, τ_p is also indicative of the rupture growth resistance. In this paper, the terms "rupture growth resistance" and "crack growth resistance" will be used synonymously.

In experiments on stick-slip failure that propagates along a simulated fault of weak junction in a large rock sample in the brittle regime, it has been found (Ohnaka et al., 1986; Ohnaka and Kuwahara, 1990) that quasistatic, leading to quasidynamic at a later time, slip failure nucleation begins to occur at a point where the resistance to rupture growth has a minimum value, and that the resistance increases with rupture growth in the nucleation zone. A recent theoretical analysis (Yamashita and Ohnaka, 1991) confirms the above experimental finding; that is, when the rupture growth resistance varies on the fault so as to increase with distance in a zone, the nucleation begins to occur at a point where the rupture growth resistance is at a minimum, and it grows stably and quasistatically in the zone. The theoretical study further shows that spatial distribution of the rupture growth resistance and the size of preexisting initial crack play an important role in creating stable and quasistatic nucleation in the brittle regime. Specifically, an increase in the critical slip displacement with distance is required for the occurrence of stable rupture growth, and the increase rate must be larger than a certain critical value (Yamashita and Ohnaka, 1991). It has thus been concluded that nonuniform distribution of the rupture growth resistance on the fault is a necessary condition for creating the sizable zone of such nucleation in the brittle regime, and that the size of the nucleation zone is governed by an inhomogeneous spatial distribution of the rupture growth resistance (Ohnaka and Kuwahara, 1990; Ohnaka, 1990; Yamashita and Ohnaka, 1991). This may be paraphrased as follows; slip-failure instability giving rise to dynamically propagating rupture over the entire fault can locally be preceded by a stable and quasistatic (leading to quasidynamic at a later time) nucleation process even in the purely brittle regime, if the rupture growth resistance is nonuniformly distributed on the fault. In addition, laboratory experiments (Ohnaka and Kuwahara, 1990) show that slip-weakening proceeds during the nucleation process. Yamashita and Ohnaka's theoretical study (1991) further shows that local dynamic instabilities do not necessarily result in a dynamic instability giving rise to rupture over the entire fault, when the rupture growth resistance on the fault varies on a local scale. Thus, it is logically concluded that the entire nucleation process prior to overall dynamic rupture can include dynamic instabilities of local to small scale. These are characteristic features of the slip-failure nucleation occurring in the brittle regime on the fault over which the rupture growth resistance is inhomogeneously distributed. Such inhomogeneity commonly exists in parts of the fault zone where a potential for earthquakes prevails. For instance, seismicity in a fault zone such as the San Andreas fault (e.g., Eaton et al., 1970) is a direct reflection of local to small-scale inhomogeneities in the brittle seismogenic layer. Since fault inhomogeneities play a key role during the nucleation, this feature must be incorporated into a physical model for the earthquake source nucleation.

With these facts and features in mind, we propose a physical model for the earthquake rupture nucleation below. The basic process during which earthquake source failure nucleates and develops to unstable dynamic rupture may be modelled conceptually as shown in Figure 2. This

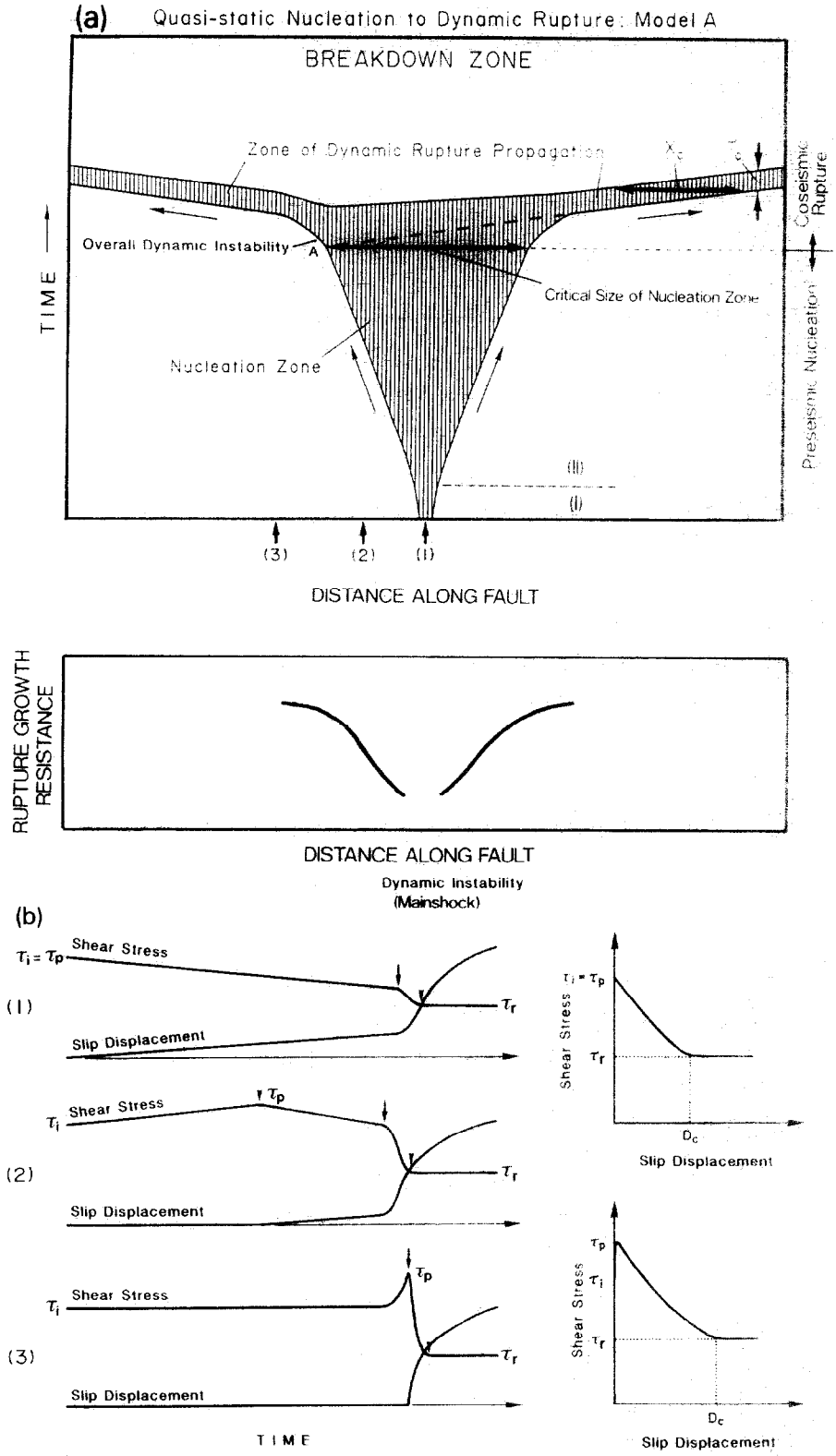

Fig. 2. A model for basic rupture nucleation, based on laboratory observations (Ohnaka and Kuwahara, 1990). The hatched portion in (a) indicates the breakdown zone where slip-weakening proceeds (see (b)). Point A in (a) denotes the onset of dynamic instability. X_c is the breakdown zone size, and T_c is the breakdown time, which is defined as the time required for the shear stress to decrease from its peak value to a residual frictional stress level. Shown on the right hand side in (b) are the slip-weakening relations, which are assumed to be the constitutive relation governing the breakdown processes throughout the quasistatic nucleation to dynamically propagating rupture. For details see text.

is based on facts found in laboratory experiments on slip failure nucleation (Ohnaka and Kuwahara, 1990; Ohnaka, 1990). Figure 2 shows how rupture grows stably with accelerating speeds from the point where a slip failure nucleus is formed to the critical point, beyond which rupture propagates unstably and dynamically at a speed close to sonic velocities. The hatched portion in Figure 2a indicates the breakdown zone where slip-weakening proceeds (see Fig. 2b). Point A in Figure 2a denotes the onset of dynamic instability. The entire process of earthquake nucleation may, in general, be composed of two successive phases: (I) quasistatic steady progression of the tip of the breakdown zone; and (II) stable but accelerating progression of the tip of the breakdown zone up to a critical state beyond which the earthquake dynamic instability occurs. The breakdown zone is defined as the zone over which local shear stress near the propagating rupture front on the fault decreases from its initial value τ_i to a residual friction stress level τ_r with ongoing slip (see Fig. 1). During such earthquake nucleation, the local shear stress decreases gradually in the breakdown zone, and at the same time the corresponding premonitory slip also proceeds in the zone, since slip-weakening occurs during the nucleation ((1) in Fig. 2). Premonitory stress (or strain) changes can also be expected to occur outside (but adjacent to) the nucleation zone; that is, local shear stresses (or the corresponding strains) on the remaining unslipped parts adjacent to the nucleation zone increase with time, because the unslipped segments must bear extra stress loads that have been sustained by the slipped parts ((2) in Fig. 2). These gradual and subsequent, accelerating changes in both stress and slip are inevitable precursors that occur locally in (or adjacent to) the zone of earthquake nucleation. However, no such precursory slip and stress degradation occur in a region distant from the nucleation zone ((3) in Fig. 2); precursory deformation and gradual stress changes are necessarily confined in (or adjacent to) the zone of earthquake nucleation. These are not products of mere speculation, but based on observed facts and physical principles (Ohnaka and Kuwahara, 1990; Ohnaka, 1990). The model suggests that it will be the key to the short-term earthquake prediction to identify where the nucleation occurs on the fault that has the potential to cause a major earthquake, because precursory signals that occur locally in the nucleation zone may be successfully detected only when the monitoring instruments are suitably installed.

That the entire nucleation process prior to overall dynamic rupture can include local dynamic instabilities leads to a more elaborate model of the earthquake nucleation during which immediate foreshocks and subsequent quiescence occur (see Fig. 3). Local dynamic instabilities that occur during a mainshock nucleation within the nucleation zone in the brittle seismogenic layer are immediate foreshocks in a strict sense, since they are generated in the process of mainshock nucleation (Fig. 3). Such local instabilities (immediate foreshocks) alone will be regarded as a manifestation of premonitory slip during the mainshock nucleation. In other words, the mainshock nucleation during which slip-weakening proceeds occurs necessarily in a zone that includes the hypocentral region of immediate foreshocks. These give a physical explanation of why immediate foreshocks are necessarily concentrated in the vicinity of the epicentres of the pending mainshocks. The mainshock nucleation in general proceeds either seismically or aseismically, because local dynamic instabilities (or foreshocks) do not necessarily occur during the mainshock nucleation. Whether or not foreshocks occur during the mainshock nucleation depends on how the rupture growth resistance varies inhomogeneously on a local to small scale on the fault (Fig. 3a). As mentioned above, the nucleation begins to occur at a location where the rupture growth resistance is at a minimum on the fault, and dynamic instability giving rise to seismic rupture occurs at a position where the energy released with further rupture growth exceeds its growth resistance (for instance, A_2 in Fig. 3a). However, the dynamic rupture may be arrested at a barrier (B_2 in Fig. 3a) where the rupture growth resistance is locally much greater, returning to stable, slow rupture growth. Once the tip of the nucleation zone penetrates through the local barrier patch of greater resistance, dynamic instabil-

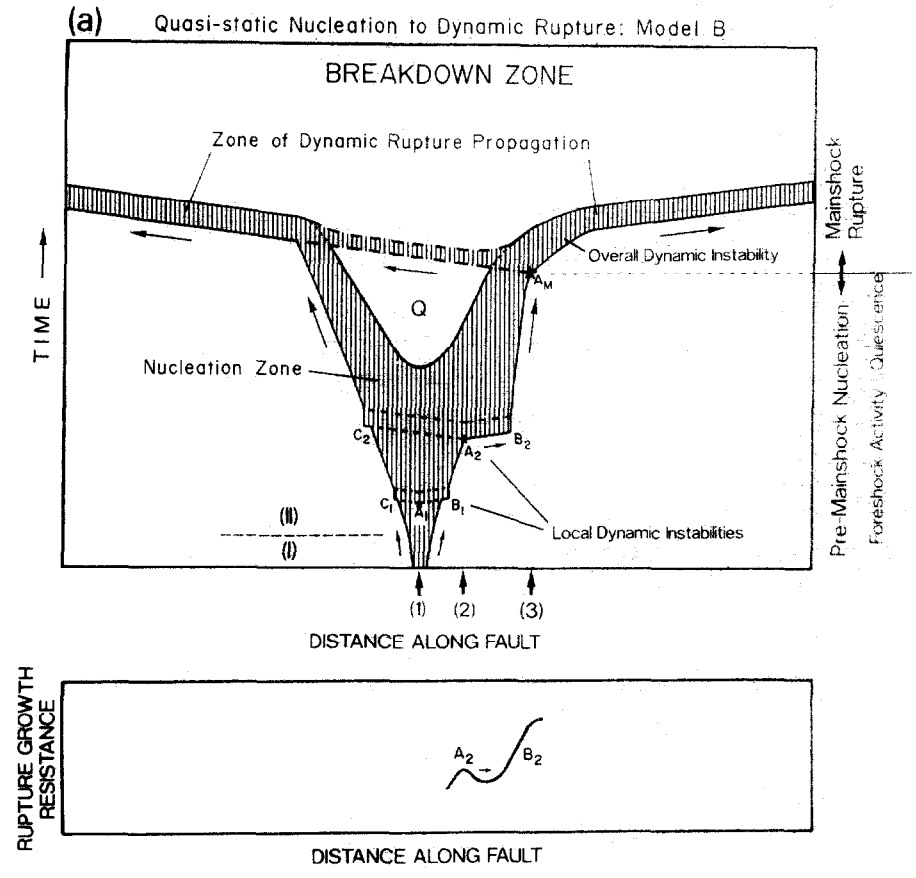
(a) Quasi-static Nucleation to Dynamic Rupture: Model B
BREAKDOWN ZONE
Zone of Dynamic Rupture Propagation
Overall Dynamic Instability
Mainshock Rupture
Pre-Mainshock Nucleation
Foreshock Activity
Quiescence
TIME
Q
Nucleation Zone
Local Dynamic Instabilities
(II)
(I)
(1) (2) (3)
DISTANCE ALONG FAULT
RUPTURE GROWTH RESISTANCE
DISTANCE ALONG FAULT

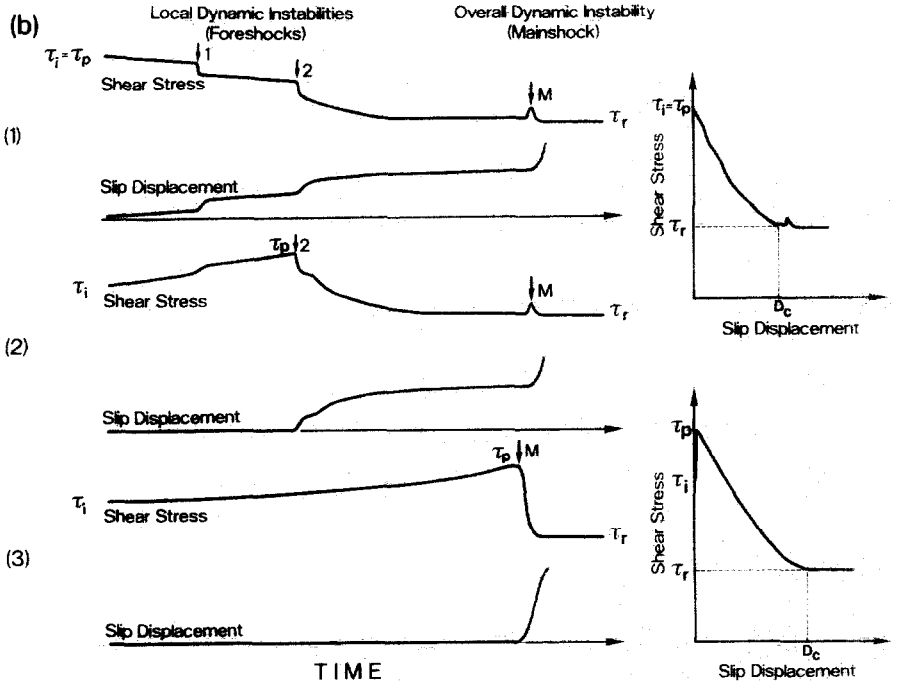
(b)
Local Dynamic Instabilities (Foreshocks)
Overall Dynamic Instability (Mainshock)
Shear Stress
Slip Displacement
(1)
(2)
(3)
TIME
Slip Displacement

ity can again occur. Thus, earthquakes located within the brittle seismogenic layer will carry foreshock activity during the nucleation, insofar as the fault is characterized by inhomogeneities of rupture growth resistance. Such a typical example is the 1978 Izu Oshima Kinkai earthquake (M_{JMA} 7.0), which carried immediate foreshock activity concentrated in the vicinity of the mainshock hypocentre at a depth of 4 km. Foreshock activity itself exemplifies local to small-scale inhomogeneities of the rupture growth resistance in the nucleation zone of natural earthquakes, which will further be discussed later.

As the nucleation proceeds, the zone where the breakdown (or slip-weakening) has finished increases (Q in Fig. 3a); this has been observed in the laboratory (Ohnaka and Yamamoto, 1984). Local dynamic instabilities can no longer occur in the zone where the stress has decreased to a residual friction stress level. This necessarily leads to a pronounced lull in foreshock activity just before the mainshock (Fig. 3), as discussed by Scholz (1988a).

3. Depth variation of rupture growth resistance

Earthquake source nucleation in the lithosphere can be computer-simulated, if the constitutive relation governing shear rupture and depth (more generally, spatial) distribution of the magnitudes of the parameters prescribing this constitutive relation are both given. As noted in the foregoing section, the breakdown zone model is virtually prescribed by the three parameters τ_p, $\Delta\tau_b$, and D_c, which are indicative of the rupture growth resistance. Therefore, depth distribution of these parameters is necessary information to simulate earthquake nucleation in the lithosphere. Whether or not a sizable zone of stable, quasistatic to quasidynamic nucleation appears prior to earthquake dynamic instability depends on how these parameters prevail nonuniformly on the fault in the lithosphere (Yamashita and Ohnaka, 1992). Spatial inhomogeneities of these parameters can be caused by the geometrical or topographical setting of the fault (zone), rock type, the presence or absence of water, ambient temperature and effective pressure at crustal depths.

For instance, fault surfaces within the brittle seismogenic layer have fractal roughness, and they exhibit self-similarity only over finite bandwidths (Aviles et al., 1987; Okubo and Aki, 1987). Scholz and Aviles (1986) showed that the slope of the power spectrum of natural rock surfaces is not constant over the wavelength band from 10 μm to 1 m. This slope change is more pronounced for the power spectra from profiles measured parallel to slip (Power et al., 1988; Power and Tullis, 1991). These observations show that a single fractal dimension is not appropriate for the fault surfaces over a wide wavelength band, and that a different fractal dimension can be calculated for each band bound by an upper and lower cutoff wavelength (Aviles et al., 1987). If this is the case, earthquake faults can have characteristic lengths given by the corner wavelengths separating the neighbouring two bands. The corner (or cutoff) wavelength in the $1-10^{-6}$ m band is particularly important because the breakdown process that occurs near the tip of propagating rupture is virtually governed by such a characteristic length scale. In fact, laboratory experiments show that the fault roughness is characterized by the cutoff wavelength λ_c of the power spectral density of the topographical roughness of the fault surface

Fig. 3. A model for earthquake rupture nucleation carrying local dynamic instabilities (or foreshocks) and a lull in foreshock activity just before the mainshock. Local dynamic instabilities are a part of the nucleation process leading to the overall dynamic rupture, when the rupture growth resistance is nonuniformly distributed on a local to small scale. The hatched portion in (a) indicates the breakdown zone where slip-weakening proceeds (see (b)). The points A_1 and A_2 in (a) denote the onset of local dynamic instabilities, and point A_M the onset of overall dynamic instability. Some dynamic instabilities may be arrested locally at barriers as shown as B_2 in (a), which are recognized as foreshocks. The portion denoted by Q is the zone where the breakdown (or slip-weakening) has finished, so that local dynamic instabilities can no longer occur there, leading to a pronounced lull in foreshock activity just before the mainshock. Shown on the right hand side in (b) are the slip-weakening relations, which are assumed to be the constitutive relation governing the breakdown processes throughout the quasistatic nucleation to dynamically propagating rupture.

(Brown and Scholz, 1985; Kuwahara et al., 1985), and that the critical slip displacement can be governed by λ_c (Kuwahara et al., 1985). The experiments further indicate that larger λ_c results in a greater rupture growth resistance and a larger size of the nucleation zone (Kuwahara et al., 1986). Rupture growth during the nucleation is greatly influenced by the existence of "asperities" or "barriers" on the fault that are local patches of greater rupture growth resistance, which might result from the geological or geometrical setting of the fault zone. Laboratory experiments (Ohnaka and Kuwahara, 1990) show that asperity patches of higher effective breakdown stress have greater critical slip displacements (see also Figs. 10 and 11). Local variation of rupture growth resistance in the brittle seismogenic layer may also be influenced greatly by local fluctuation of pore water pressure.

By contrast, overall depth variation of the rupture growth resistance in the lithosphere results from the nonuniform distribution of ambient temperature and effective pressure at crustal depths. Earthquake nucleation and the shallow depth confinement of the seismicity (e.g., Sibson, 1982; Tse and Rice, 1986) are likely governed by overall depth variation of the parameters indicative of the rupture growth resistance. It is thus crucial to know the overall depth distribution of these parameters. In spite of its importance, however, depth variation of those parameters, in particular that of the critical slip displacement, is still not fully understood. Mechanical properties of rock at mid-crustal depths (roughly 10 to 25 km) are in general characterized by semibrittleness, because the lithostatic pressure in this depth interval ranges from about 300 to 750 MPa and the temperature from roughly 300 to 750°C, and because the mechanical behaviour for crystalline rocks in these pressure and temperature ranges is transitional in nature from brittle behaviour to crystal plastic deformation (e.g., Carter and Kirby, 1978). Thus, the semibrittleness is essential when the variation of the rupture growth resistance at mid-crustal depths is discussed. The portion shallower than this transition layer may generally be characterized as brittle, and the strength of this shallow portion may be represented by friction on preexisting faults prevalent in that portion (e.g., Sibson, 1982, 1984), while the deeper portion may be characterized as plastic at a geological strain rate, as will be discussed later. We thus postulate a three-layer fault zone model composed of the brittle upper layer, the plastic lower layer, and the intervening transitional (or semibrittle) layer (e.g., Scholz, 1988b). Shear resistance in the brittle upper layer is considered to obey the rock friction law (Byerlee, 1978), and flow resistance in the plastic lower layer to obey the steady-state flow power law (e.g., Carter, 1976). It is not known for any material, however, what specific law the shear resistance obeys in the intervening transitional layer. Therefore, this must be solved to estimate depth distribution of shear resistance in the lithosphere. Thus, we here first evaluate quantitatively the effects of pressure and temperature on the shear resistance of Westerly granite in the transitional regime, and then estimate how the parameters indicative of the rupture growth resistance vary with depth, by considering the effects of pressure and temperature to be derived from available laboratory data so far published.

3.1. Peak shear resistance

The breakdown strength for intact Westerly granite at elevated temperatures under confining pressures has been experimentally studied by Griggs et al. (1960), Stesky et al. (1974), and Wong (1982a), although the post-failure behaviour at elevated temperatures was investigated by Wong (1982a) alone. These experiments were performed at strain rates ranging from 5×10^{-4}/s to 10^{-5}/s. The effect of strain rate is negligible in the range 5×10^{-4}/s to 10^{-5}/s (Wong, 1982a), so that this effect is disregarded in the present analysis. Using these data makes it possible to evaluate the effects of temperature and normal stress on the peak shear resistance for Westerly granite in the transitional regime.

The shear resistance to failure is in general pressure-dependent but temperature-insensitive in the purely brittle regime, while the shear resistance to flow is temperature-dependent but pressure-independent in the purely plastic regime. In the transitional regime from brittle failure to

plastic deformation, however, it is reasonable to presume that the shear resistance depends on both pressure and temperature, because brittle behaviour of crystalline rocks should combine with thermally activated plastic flow processes to the fracture in the transitional regime (e.g., Carter and Kirby, 1978). We assume that the effects of pressure and temperature on the peak shear strength τ_p are mutually independent and separable in the transitional (or semibrittle) regime, and under this assumption, τ_p may be expressed as

$$\tau_p(\sigma_n, T) = f(\sigma_n) g(T) \tag{1}$$

where $f(\sigma_n)$ and $g(T)$ are functions of the normal stress σ_n across the fracture plane and temperature T, respectively. When T is held constant at a constant strain rate, the peak shear strength τ_p is a function of σ_n alone, and practically, τ_p at $T = T_0$ is well approximated by a linear form:

$$\tau_p(\sigma_n, T_0) = \tau_{p0}(\sigma_n) = c_0 + c_1 \sigma_n \tag{2}$$

where c_0 and c_1 are constants. This is what is called the Coulomb equation, and is confirmed by the above experimental data, from which we have $c_0 = 135.7$ MPa and $c_1 = 0.750$ for data in the temperature range from room temperature to 150°C. In this temperature range, mechanical properties of Westerly granite are highly temperature-insensitive. In fact, Wong (1982a) concluded that the pressure-dependence at 150°C is almost identical to that at room temperature. Equation 2 shows that the breakdown shear strength $\tau_{p0}(\sigma_n)$ at room temperature or below 150°C is linearly related to the normal stress. Figure 4 shows a plot of $\tau_p(\sigma_n, T)$ divided by $\tau_{p0}(\sigma_n)$ against the reciprocal of absolute temperature T for Westerly granite: dots indicate data from Wong (1982a, b), circles those from Stesky et al. (1974), and triangles from Griggs et al. (1960). We find from Figure 4 that all the data points obtained at various confining pressures by different authors are aligned along a single curve, given experimental errors inevitably involved in those data, and the effect of temperature can be represented by the following equation:

$$\frac{\tau_p(\sigma_n, T)}{\tau_{p0}(\sigma_n)} = \frac{g(T)}{g(T_0)} = 1 - \left[\cosh\left(\frac{C_2}{T}\right) + \left(\frac{C_1}{C_2}\right) \sinh\left(\frac{C_2}{T}\right)\right] \times \exp\left(-\frac{C_1}{T}\right) \tag{3}$$

where C_1 and C_2 are constants, and $C_1/C_2 > 1$. Equation 3 seems well fitted to the data points over a wide range of temperature from the brittle to semibrittle regime, when $C_1 = 2000$°K and $C_2 = 50$°K (curve A in Fig. 4). A theoretical explanation for this model function will not be given here, since this is beyond the scope of the present paper. Figure 4 confirms earlier authors' conclusion (e.g., Tullis and Yund, 1977; Wong, 1982a) that the effect of temperature $g(T)$ is insignificant below 300°C for dry Westerly granite, indicating that dry Westerly granite in this temperature range is in the brittle regime. Equation 3 combined with eq. 2 represents the effects of σ_n and T on the breakdown shear strength τ_p in the brittle to semibrittle regime.

Experimental data on friction for Westerly granite (Stesky et al., 1974) show that frictional strength is virtually independent of temperature

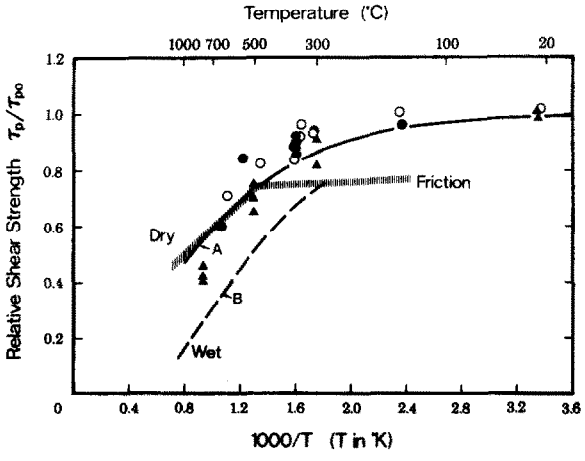

Fig. 4. A plot of $\tau_p(\sigma_n, T)/\tau_{p0}(\sigma_n)$ against $1/T$ for Westerly granite. Triangles show data from Griggs et al. (1960), circles those from Stesky et al. (1974), and dots from Wong (1982a, b). The continuous curve A indicates eq. 3 with $C_1 = 2000$°K and $C_2 = 50$°K. The broad shaded line denotes Stesky's law at a given sliding rate (10^{-4} cm/s). The dashed curve B indicates the relation between $\tau_p(\sigma_n, T)/\tau_{p0}(\sigma_n)$ and $1/T$ in a wet environment where the temperature at which the shear strength for intact rock becomes equal to frictional shear resistance has been assumed to be lowered by 220°C.

below 500°C, above which the frictional strength decreases with increasing temperature. Stesky (1978) derived a law for frictional sliding in Westerly granite at high temperatures of the form:

$$\dot{\delta} = \dot{\delta}_0 \exp\left(\frac{\tau}{\tau_0}\right) \exp\left(-\frac{Q}{RT}\right) \quad (4)$$

where $\dot{\delta}$ is the sliding rate, τ is the applied shear stress, Q is the activation energy for frictional sliding, R is the gas constant, $\dot{\delta}_0$ and τ_0 are constants. Stesky (1978) estimated that $\tau_0 = 5$ MPa and $Q/R = 4.28 \times 10^4$°K in the temperature range 500°C to 700°C, and $\tau_0 = 1$ MPa and $Q/R = 1.51 \times 10^4$°K below 500°C. This is denoted by the broad shaded line in Figure 4 as predicted from this law for frictional sliding at a given sliding rate (10^{-4} cm/s), where $\dot{\delta}_0$ has been estimated to be 7.9×10^{-10} cm/s by assuming that $\tau = 319$ MPa at $\dot{\delta} = 10^{-4}$ cm/s and $T = 823$°K (Stesky, 1978). Figure 4 indicates that above 500°C, frictional shear resistance is equal to the breakdown shear strength for intact rock, while below 500°C, frictional resistance is significantly lower than the strength of intact rock (Stesky et al., 1974; Stesky, 1978). Above 500°C, both breakdown shear strength for initially intact rock and frictional resistance decrease with increasing temperature along the same curve. This is probably because "welding" of the compressed fault surfaces, which makes the real area of contact equal to the nominal area, occurs above 500°C (Stesky, 1978). Crystal plastic deformation near the fault surfaces is necessary to bring about such "welding". Stesky (1978) detected plasticity in quartz at about 500°C, and Tullis and Yund (1977) observed at the strain rate of 10^{-6}/s that quartz in dry Westerly granite begins to deform plastically at about 300°C, and that plastic deformation of feldspar begins to occur at 500°C.

The depth variation of peak shear resistance in the lithosphere has been estimated to the first-order approximation by considering the change of deformation mechanism from pressure-sensitive brittle frictional sliding at shallow depths to temperature-sensitive aseismic ductile flow at greater depths (e.g., Sibson, 1982, 1984). This model, which provides an upper bound to shear resistance profiles in the lithosphere, is based on the

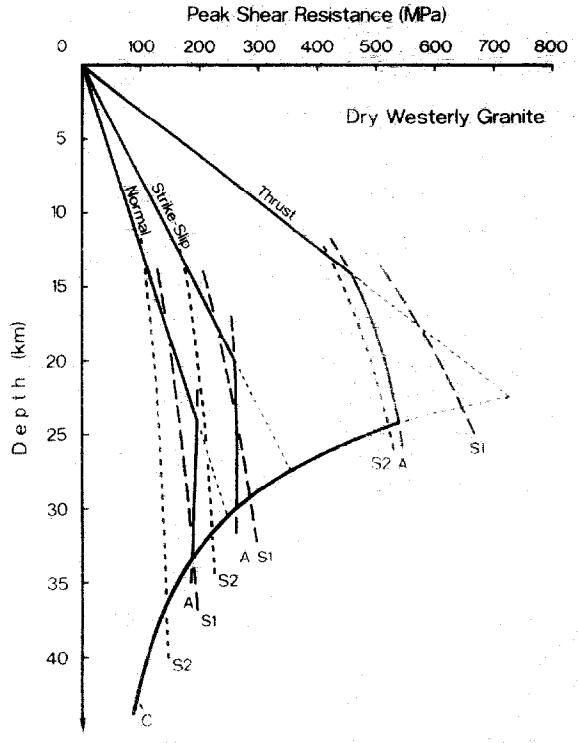

Fig. 5. Depth variation of the shear resistance for different faulting modes for dry Westerly granite. Thick lines labelled *A* at mid-crustal depths indicate the shear resistance estimated from eq. 3. Dashed curves labelled *S1* and *S2* indicate the shear resistance estimated from Stesky's law (eq. 4) with different sliding rates of 10^{-4} cm/s and 10^{-9} cm/s, respectively. Curve *C* indicates the extrapolation of the Hansen and Carter (1982) law to the geological strain rate of 10^{-14}/s.

rock friction law (Byerlee, 1978) in the brittle regime and the power law creep flow (e.g., Carter, 1976) below in the plastic regime. The frictional shear resistance increases with depth in the brittle regime, below which it falls off exponentially according to the creep flow law with increasing depth, since temperature increases roughly linearly with depth. The model is thus characterized by a sharp brittle–plastic transition at the base of the brittle seismogenic zone (Sibson, 1982, 1984). Such a sharp brittle–plastic transition would considerably be smoothed, given the existence of a transitional layer (e.g., Scholz, 1988b). A more realistic depth profile of the shear resistance can be estimated if the effects of normal stress and temperature in the transition layer from the brittle to plastic regime are considered. Figure 5 shows the depth variation of peak shear resis-

tance for different faulting modes for dry Westerly granite. Following Sibson (1982, 1984), we have assumed a friction law of the type:

$$\tau_f = \mu \sigma_n^{eff} \tag{5}$$

where τ_f is the frictional shear resistance, μ is the frictional coefficient and σ_n^{eff} is the effective normal stress acting on the fault. Byerlee's law for rock friction (Byerlee, 1978) can be approximated by eq. 5 with $\mu = 0.75$. The constitutive steady-state flow law in the ductile regime (e.g., Carter, 1976) is of the form:

$$\dot{\varepsilon} = A(\sigma_1 - \sigma_3)^n \exp\left(-\frac{Q}{RT}\right) \tag{6}$$

where $\dot{\varepsilon}$ is the strain rate, A, n and Q are constants. Whether or not steady-state flow takes place in the lower part of the crust depends on the assumed rock type, temperature, strain rate, and presence or absence of water. We hereafter simply assume the crust to consist of Westerly granite (or mechanically equivalent rocks), and the temperature gradient to be of 30°C/1 km depth. This temperature gradient is likely to be most appropriate in the Izu-Oshima region (Bodri et al., 1989), where the 1978 Izu Oshima Kinkai earthquake occurred, and the nucleation process of this particular earthquake will be discussed later. Sibson (1982, 1984) argued that quasiplastic strain rates of 10^{-11}/s–10^{-12}/s are appropriate for fault systems such as the San Andreas transform plate boundary at depth. The strain rates of 10^{-11}/s–10^{-12}/s correspond to a slip rate of about 3 cm/yr across fault zone widths of 0.1 km–1.0 km (Sibson, 1984). We will later discuss the nucleation process of intraplate earthquakes in Japan, for which the strain rate of an order of 10^{-11}–10^{-12}/s is too high. Matsuda (1977) estimated long-term average slip rates for active faults on land in Japan, which are considered to be typical intraplate earthquake faults. The average slip rates estimated by Matsuda fell in the range of 1–0.01 mm/yr, which corresponds to the strain rates ranging from 3×10^{-12}/s to 3×10^{-16}/s if the width of those active fault zones is assumed to be in the range of 10 m to 1 km. Accordingly, we here adopt a value of 10^{-14}/s as a representative geological average strain rate for intraplate earthquake fault systems. For steady-state plastic flow to take place, the ratio of the ambient to the melting temperature T/T_m of the rock undergoing creep must generally exceed 0.5 (Carter, 1976); however, this value becomes lower at a lower strain rate. Tullis and Yund (1977) observed for dry Westerly granite at a laboratory strain rate of 10^{-6}/s that the transition from dominantly microcracking to dominantly plastic flow occurs at about 300°–400°C for quartz and 550°–650°C for feldspar. This observation suggests that dry Westerly granite may deform completely plastically above 500°C at a geological strain rate of 10^{-14}/s. If this is the case, and if Hansen and Carter's (1982) flow law ($A = 2.6 \times 10^{-9}$ MPa^{-n} s^{-1}, $n = 3.4$, and $Q = 33.3$ kcal mol^{-1}) for Westerly granite can be extrapolated to the geological strain rate of 10^{-14}/s, it may be justified to estimate the steady-state plastic flow resistance (or at least its upper bound) at the strain rate of 10^{-14}/s, by using the above flow law parameters.

We assume that the shear resistance τ_{tect} at crustal depths is given by:

$$\tau_{tect} = \min\{\tau_f, \tau_{flow}, \tau_p\} \tag{7}$$

where τ_{flow} is the plastic flow shear resistance at the geological strain rate of 10^{-14}/s, and τ_p is the shear strength in the transitional regime. If the shear resistance in the transitional regime is assumed to deform according to eq. 3 with $C_1 = 2000$°K and $C_2 = 50$°K, the depth variation of peak shear resistance τ_{tect} for different faulting modes under a dry condition is estimated as shown by the thick lines labelled A in Figure 5. For strike-slip faulting, we have considered the particular case where the vertical stress $\sigma_v = \sigma_2 = (\sigma_1 + \sigma_3)/2$ (σ_1, σ_2, and σ_3 being the maximum, intermediate, and minimum principal compressive stresses, respectively). In this estimate, the effect of strain rate in the transitional regime has been disregarded, since its quantitative effect is not known. Qualitatively, however, the shear resistance in the transition regime should be more reduced at the geological strain rate of 10^{-14}/s than the curve shown in Figure 5, and in this sense the present estimate may be an upper bound in the regime. A similar estimate can be made using Stesky's law (eq. 4), from which the effect

of strain rate (or slip rate) in the transitional regime can be evaluated. If the shear resistance is assumed to deform according to Stesky's law (eq. 4), the shear resistance profiles for different faulting modes around the transition depth are represented by the broken curves (S1 for slip rate of 10^{-4} cm/s, and S2 for 10^{-9} cm/s) in Figure 5, where it has been assumed that the law can be extrapolated to the geological slip rate of 10^{-9} cm/s (= 0.3 mm/yr). We find from Figure 5 that the shear resistance peak for each faulting mode is smoothed under a dry condition, and that the effect of strain rate (or slip rate) can be considerable in the transition regime.

In wet environments, the breakdown strength of granitic rock decreases due to both mechanical and chemical effects. Mechanical effect of water on strength can be evaluated by a law of effective stress (e.g., see Jaeger and Cook, 1976; Paterson, 1978). However, chemical effects on strength are difficult to assess quantitatively, although it is a well known fact that the presence of water reduces the breakdown strength significantly due to stress corrosion (e.g., Atkinson, 1987) and enhances plasticity due to hydrolytic weakening for silicate minerals (Griggs and Blacic, 1965; Griggs, 1967; Blacic, 1975; Kekulawala et al., 1978). High pressure enhances hydrolytic weakening (Tullis and Yund, 1980), and stress corrosion cracking is enhanced by temperature (Meredith and Atkinson, 1985). Wong (1982a) observed that the effect of water on strength reduction is more pronounced at elevated temperatures than at room temperature. We thus anticipate that the shear resistance at higher temperatures would more significantly be lowered in the presence of water. Tullis and Yund (1980) demonstrated that water significantly lowers the transition temperature of quartz and feldspar minerals from microcracking to dislocation glide and climb. With this in mind, we assume that the temperature at which the shear strength for intact rock becomes equal to frictional shear resistance is lowered by 220°C in wet environments (curve B in Fig. 4). In addition, the parameter c_0 in eq. 2 is related to "cohesion" on fracture surfaces, so that this parameter will be influenced by the chemical action of water. As an example, the case where cohesion for wet

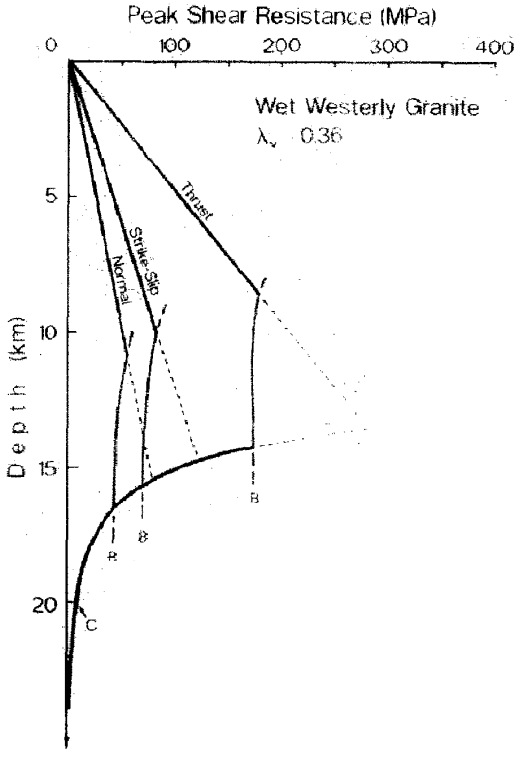

Fig. 6. Depth variation of the shear resistance for different faulting modes for Westerly granite at hydrostatic pore water pressure. Curves labelled *B* denote the case where critical temperature at which the shear strength for intact rock becomes equal to frictional shear resistance is lowered by 220°C in a wet environment, and where cohesion for wet Westerly granite is weakened by 30% as compared with that for dry Westerly granite. Curve *C* indicates the extrapolation of the Hansen and Carter (1982) law to the geological strain rate of 10^{-14}/s.

Westerly granite is weakened by 30% of that for dry Westerly granite at hydrostatic pore water pressure (the ratio of the fluid pressure to the lithostatic load $\lambda_v = 0.36$) is shown in Figure 6 (curves B), in which $A = 1.9 \times 10^{-3}$ MPa^{-n} s^{-1}, $n = 1.5$, and $Q = 32.8$ kcal mol^{-1} for a flow law (eq. 6) have been assumed for wet Westerly granite (Hansen and Carter, 1982). The tectonic strain rate of 10^{-14}/s has also been assumed here, and at this strain rate wet granite is assumed to deform plastically below the transition depth. An extrapolation of the Hansen and Carter law to the geological strain rate of 10^{-14}/s may give an upper bound of plastic flow resistance at that strain rate. We find also in this case that the shear resistance around the transition depth is

smoothed for different faulting modes. The level of shear resistance in the transitional regime (curves B in Fig. 6) depends on the assumed "cohesion strength". If cohesion is weakened in wet environments by less than 30%, the level of shear resistance in the transitional regime becomes higher than the level shown in Figure 6, and if cohesion is more weakened, the shear resistance level is more lowered in the regime. The strain rate effect in the transitional regime in wet environments is difficult to assess quantitatively, so that this has been disregarded in Figure 6 (the portion denoted by B). Qualitatively, if this effect is considered, the shear resistance in the transitional regime will be more reduced at the geological strain rate of 10^{-14}/s than the curves shown in Figure 6.

3.2. Critical slip displacement

Figure 7 shows a plot of the shear fracture energy versus temperature for initially intact Westerly granite. Data are taken from table 2 of Wong (1982b). This figure shows that the shear fracture energy does not depend on temperature over a broad range from room temperature to 950°K; it can be regarded as constant (2.6×10^4 J/m^2) in this range. This finding will be used later as a constraint when the effect of temperature on the critical slip displacement is evaluated for Westerly granite. The mode of rock fracture is in general shear under compressive stresses, and

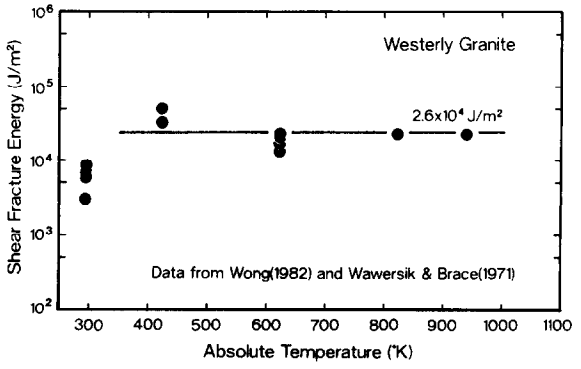

Fig. 7. A plot of shear fracture energy against temperature for initially intact dry Westerly granite. Data from Wawersik and Brace (1971) and Wong (1982b).

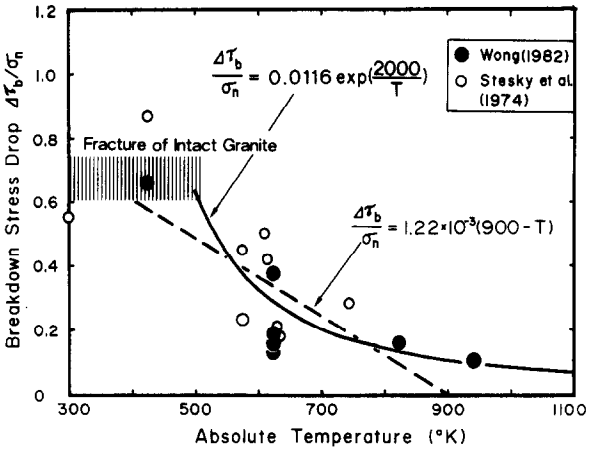

Fig. 8. A plot of $\Delta\tau_b/\sigma_n$ against temperature for initially intact dry Westerly granite. Data from Stesky et al. (1974) and Wong (1982b).

both breakdown shear strength and residual friction stress depend on the normal stress across the fault. Thus, the breakdown stress drop $\Delta\tau_b$ is a function of σ_n. In the semibrittle regime, $\Delta\tau_b$ is not only a function of σ_n, but also a function of T and $\dot{\varepsilon}$. The effect of $\dot{\varepsilon}$ is considered negligible in the limited range of strain rate 10^{-4}–10^{-5}/s, so that the effect of $\dot{\varepsilon}$ is not possible to reveal by use of the present data set, and this effect is disregarded in the analysis below. We assume that $\Delta\tau_b$ is expressed a follows:

$$\Delta\tau_b(\sigma_n, T) = f'(\sigma_n)g'(T) \tag{8}$$

where $f'(\sigma_n)$ and $g'(T)$ are functions of σ_n and T, respectively. We here further assume that the effect of σ_n, $f'(\sigma_n)$, is approximated by a linear form of σ_n. Under the above assumptions, $\Delta\tau_b/\sigma_n$ is a function of T alone. Data available for the present purpose on Westerly granite so far published (Stesky et al., 1974; Wong, 1982a, b) show clearly a tendency (see Fig. 8) that $\Delta\tau_b/\sigma_n$ decreases with increasing temperature above 300°C, whereas $\Delta\tau_b/\sigma_n$ may be considered roughly constant at lower temperatures. This latter consideration would be reasonable when the shear failure stress and the residual friction stress in the brittle regime increase approximately linearly with the normal stress acting on the fault. It seems obvious that $\Delta\tau_b/\sigma_n$ is a function of temperature above 300°C, and the functional form in this

temperature range may reasonably be assumed to be:

$$\frac{\Delta\tau_b}{\sigma_n} = A \exp\left(\frac{Q}{RT}\right) \quad (9)$$

where A and Q are constants, given thermally activated processes involved in the semibrittle regime. If this exponential form is assumed for the data by Stesky et al. (1974) and Wong (1982a, b), we have $A = 0.0116$ and $Q/R = 2000$°K (see Fig. 8). However, the simplest fit to the data is a linear relation, and if a linear relationship is assumed for the same data set, just to obtain a purely empirical relationship between $\Delta\tau_b/\sigma_n$ and T as a first approximation, we have (Fig. 8):

$$\frac{\Delta\tau_b}{\sigma_n} = 1.22 \times 10^{-3}(900 - T) \quad (10)$$

where T is measured in °K.

It follows from the above results that D_c should increase with increasing temperature, since the shear fracture energy is given roughly by the product of $\Delta\tau_b$ and D_c. This should be verified independently by experimental data. At present, there is only one set of available experimental data on D_c at elevated temperatures for initially intact Westerly granite, published by Wong (1982b), and this data set is used for checking the effect of T on D_c. Figure 9 shows a plot of D_c against T, where D_c is divided by $D_{co} = 0.11$ mm which is assumed to be the critical slip displacement at 573°K (= 300°C) for initially intact Westerly granite. Numerical values adjacent to individual data points in Figure 9 denote the resolved normal stress across the fault. We notice from Figure 9 that D_c has nearly the same values at a temperature of 630°K, despite considerable differences in the resolved normal stress, showing that D_c is insensitive to the normal stress at this temperature. Above about 300°C, D_c increases sharply with T (dots in Fig. 9), while below 300°C, D_c seems to be insensitive to T but depend pronouncedly on σ_n (circles in Fig. 9). Note that the two data points denoted by circles in Figure 9 do not conform to a general trend of the D_c versus T relation in the higher temperature range, and that they are rather sensitive to σ_n. This is in sharp contrast with the normal stress-insensitivity

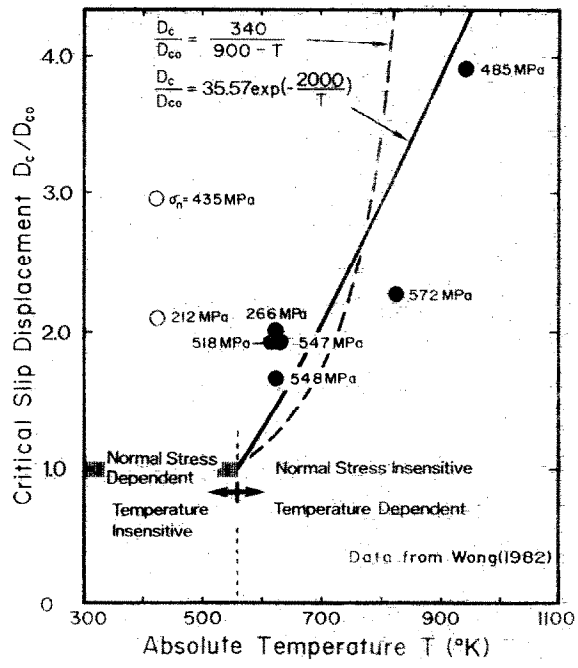

Fig. 9. A plot of the critical slip displacement against temperature for initially intact dry Westerly granite. $D_{co} = 0.11$ mm is assumed to be the critical slip displacement at 300°C. Numerical values adjacent to data points denote the resolved normal stress across the fault. Data from Wong (1982b).

in the higher-temperature range. It can thus be concluded that D_c is temperature-dependent but normal stress-independent above about 300°C, below which D_c is normal stress-dependent but temperature-insensitive.

The observation that D_c increases with increasing T above 300°C, while D_c is insensitive to T does not contradict a similar observation made for rock friction (Lockner et al., 1986). When sliding velocity is changed suddenly, frictional stress changes in the same sense as the velocity change, and then evolves with further sliding displacement towards a steady-state level. The sliding displacement d_r required for velocity-induced transient friction to reach a steady-state level has a physical meaning similar to D_c. Lockner et al. (1986) experimentally studied the effect of temperature on d_r for artificial granite gouge layers on saw-cut Westerly granite surfaces, and they observed that d_r tended to increase with increasing temperature. More specifically, their data, though scattered, seem to indicate that d_r is insensitive to temperatures below 300°–400°C,

while it increases with increasing temperature above 300°–400°C (see fig. 6 in their paper).

The limited number of available data makes it impossible to determine uniquely from the observed data alone what specific relation should hold between D_c and T. Here, the relation will be inferred under the following two assumptions: (1) the shear fracture energy is temperature-independent, and (2) the relation between breakdown stress drop and temperature obeys eq. 9 or 10. If relation 9 is adopted, we have for the relation between D_c and T:

$$\frac{D_c}{D_{co}} = A \exp\left(-\frac{B}{T}\right) \tag{11}$$

where $A = 35.57$, $B = 2000$, and T is measured in °K. If, however, linear relation 10 is assumed, D_c is reciprocally related to T as:

$$\frac{D_c}{D_{co}} = \frac{A}{B - T} \tag{12}$$

where $A = 340$, $B = 900$, and T is measured in °K. Wong (1982a) concluded that temperature stabilizes postfailure behaviour. Since the stabilizing effect should be effected by an increase in D_c, eq. 11 or 12 may be a quantitative expression of Wong's above qualitative conclusion.

We have tentatively concluded that below 300°C, the critical slip displacement is normal stress-sensitive but temperature-insensitive. If this is true, the normal stress-dependence of the critical slip displacement must be verified directly from actual laboratory data obtained within this particular temperature range. This has been checked by using available data published, and the result is shown in Figure 10, which is a plot of D_c versus $\Delta\tau_b$ for data on initially intact Westerly granite obtained at room temperature and at 150°C. The data are taken from table 2 of Wong (1982b) (in which data at room temperature are from Wawersik and Brace, 1971). For Wawersik and Brace's data, the resolved normal stress was not possible to calculate because of unknown fracture angles. In Figure 10, therefore, D_c is plotted not versus σ_n, but versus $\Delta\tau_b$. Since $\Delta\tau_b$ generally increases with increasing σ_n in the temperature and confining pressure ranges of the present concern, we can conclude from Figure 10 that D_c increases with increasing σ_n at the lower temperatures. The relation between $\Delta\tau_b$ and D_c for Westerly granite shown in Figure 10 is found empirically to be of the form:

$$D_c = D_{co}\left(\frac{\Delta\tau_b}{\Delta\tau_{bo}}\right)^K \tag{13}$$

where D_{co}, $\Delta\tau_{bo}$ and K are constants. Note that there is a positive correlation between D_c and $\Delta\tau_b$.

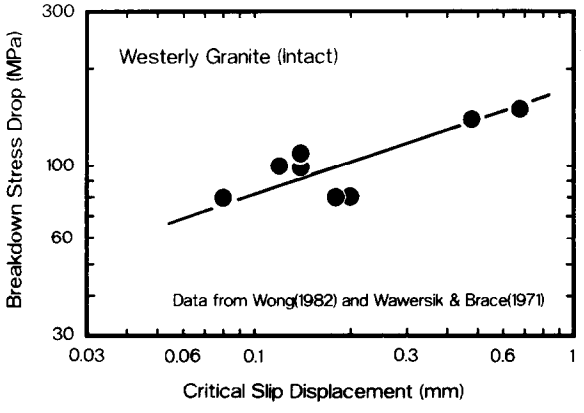

Fig. 10. A relation between the critical slip displacement and the breakdown stress drop for initially intact dry Westerly granite. Data in the range from room temperature to 150°C, taken from Wawersik and Brace (1971) and Wong (1982b).

We have concluded above that D_c depends on σ_n for initially intact Westerly granite. One may argue that this does not necessarily guarantee the normal stress-dependence of D_c for stick-slip that occurs on the precut fault. However, this also seems true in the case of stick-slip shear failure propagating along the precut fault; Figure 11 indicates a positive correlation observed between D_c and $\Delta\tau_b$ for data on stick-slip. Figure 11 shows a plot of $\Delta\tau_b$ during stick-slip failure versus D_c normalized to λ_c. The data are taken from our previous experiments on stick-slip failure in the Tsukuba granite sample (Ohnaka et al., 1987; Ohnaka and Kuwahara, 1990; unpublished data). $\Delta\tau_b$ is proportional to σ_n for stick-slip along a precut fault. It can thus be concluded from Figure 11 that D_c increases with increasing σ_n. This is the same conclusion as has been obtained for initially intact Westerly granite. Since λ_c is the cutoff wavelength of the power spectral density for geometrically *unmated* surfaces, λ_c

here is independent of the applied normal stress. D_c is proportional to λ_c (Kuwahara et al., 1985). These facts lead to the conclusion that the proportionality constant is a function of the applied normal stress, that is, $D_c/\lambda_c = m(\sigma_n)$, and that the magnitude of the proportionality constant $m(\sigma_n)$ increases with increasing σ_n. The observed data in Figure 11 indicate that $m(\sigma_n) < 1$.

Why does D_c increase with increasing normal stress? The reason for this may be that the breakdown of contacting portions on the precut fault depends on both local strength and geometrical size of the mated parts; for instance, large slip displacement will be required for a single large asperity to break down. At high normal stresses, a number of local asperities gets included in a single breakdown zone (cf. Fig. 12), because larger deformation of the asperities that are in contact, causes more asperities to get in contact at a higher normal stress. Thus, the overall breakdown zone consists of the combination of the breakdowns of a number of local asperities (Fig. 12), and the critical displacements d_c for these local asperities' breakdown added together make the critical slip displacement D_c for the overall breakdown. Thus, D_c becomes greater at a higher normal stress. The critical displacement d_c of each local asperity's breakdown should decrease with increasing normal stress. In fact, laboratory experiments (Ohnaka et al., 1986) indicate that the breakdown zone of a local asperity decreases with increasing normal stress, and this local breakdown is responsible for generating high-frequency seismic radiation (Ohnaka et al., 1986; Ohnaka and Yamashita, 1989). Scholz (1988c) showed that geometrically unmated fractal surfaces can develop a characteristic length in their contact, when they are in contact under a normal load, and he predicted theoretically that the critical slip displacement should be inversely propor-

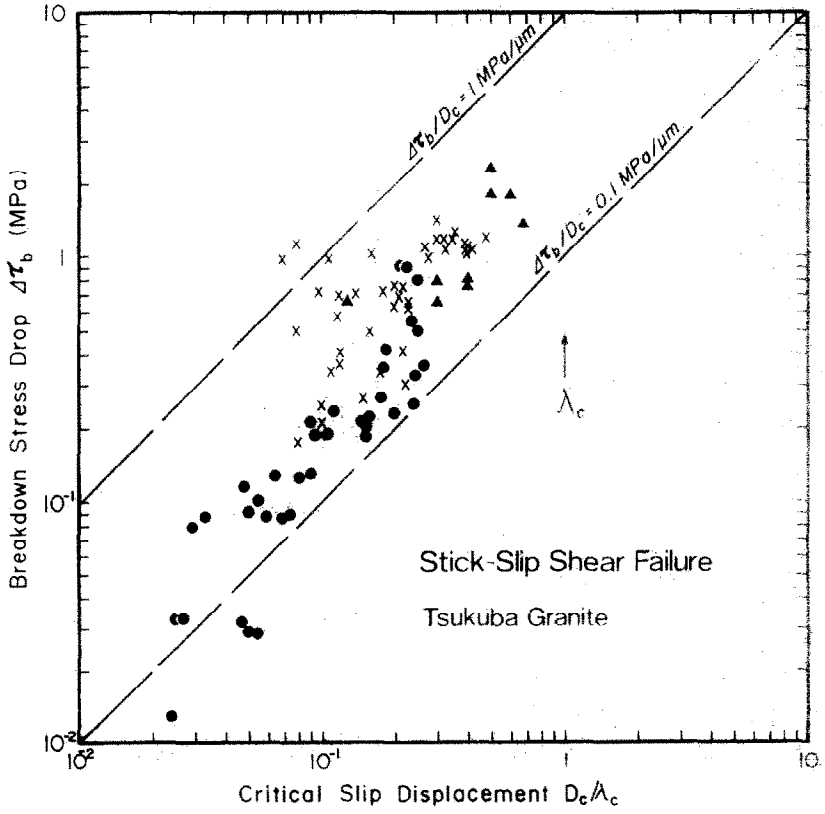

Fig. 11. A relation between the critical slip displacement and the breakdown stress drop for stick-slip along a precut fault in Tsukuba granite at room temperature. Data are from Ohnaka et al. (1987), Ohnaka and Kuwahara (1990) and unpublished data. λ_c is the cutoff wavelength of the power spectral density of the topographical roughness of the sliding surface.

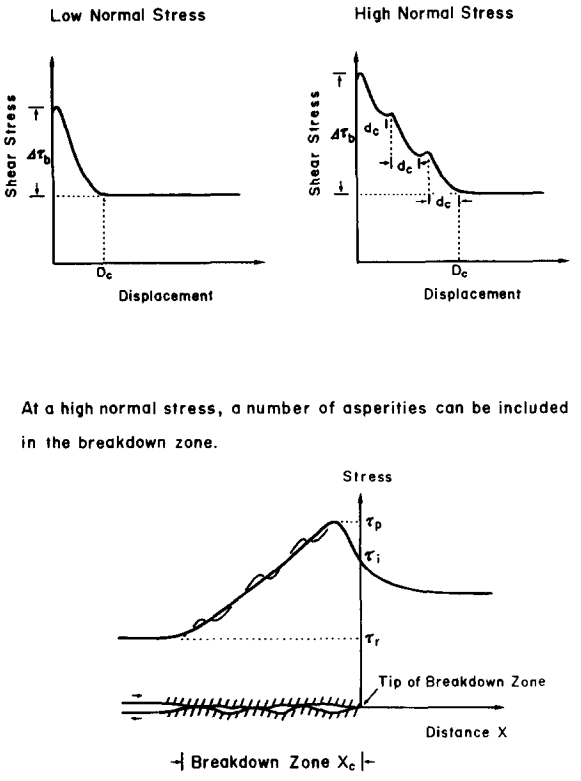

Fig. 12. A conceptual model for the breakdown zone that includes a number of local asperities. D_c represents the critical slip displacement for overall breakdown, and d_c denotes the critical slip displacement for each local breakdown. τ_p is the peak shear stress, τ_i is the shear stress on the verge of slip at a crack-tip, τ_r is the residual friction stress, and $\Delta\tau_b = \tau_p - \tau_r$.

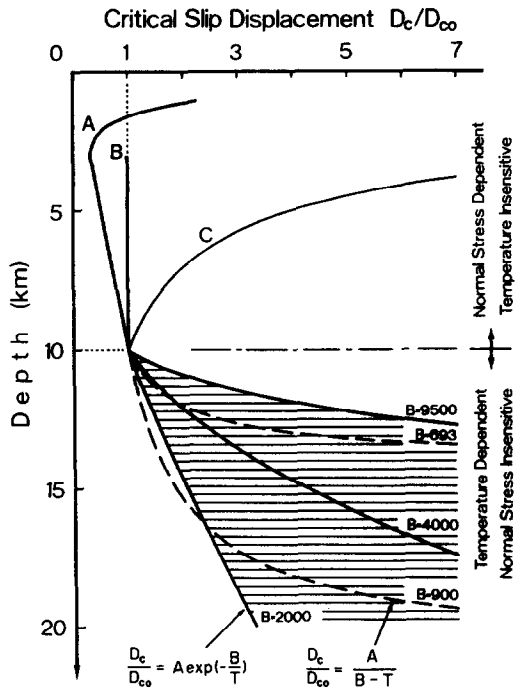

Fig. 13. Depth variations of the critical slip displacement for a given geothermal gradient (30°C/km). The continuous curves at depths greater than 10 km are obtained from eq. 11, and the dashed curves from eq. 12. Also shown are three models for which D_c has different depth variations at depths shallower than 10 km. For models *A*, *B* and *C* see text.

tional to the square of applied normal stress. The critical displacement he theoretically predicted, may correspond to that of the above local breakdown.

Using the above results makes it possible to crudely estimate the variation in the critical slip displacement with crustal depth for a given geotherm. The depth variation of D_c relative to the value of D_c at 10 km depth is shown in Figure 13, where a linear geothermal gradient of 30°C/km has been assumed. The transition depth at which D_c changes from the pressure-sensitive to temperature-sensitive regime depends on a given geothermal gradient. An increase or decrease in geothermal gradient causes the transition to migrate upward or downward, respectively. In this model, D_c at depths greater than 10 km has been assumed to increase with depth according to eq. 11, where B is taken as a parameter (thick continuous curves in Fig. 13). Increasing water content enhances plasticity (Griggs and Blacic, 1965; Griggs, 1967; Blacic, 1975; Kekulawala et al., 1978), and hence the constants of A and B in eq. 11 will depend on water content. Three cases with representative values of the parameter $B = 2000$, 4000 and 9500°K are shown in Figure 13. The case $B = 2000$°K is what has been inferred from laboratory data under a dry condition. We thus anticipate that the value of B at wet conditions is much larger than 2000°K; the cases for which $B = 4000$°K and 9500°K shown in Figure 13, may correspond to those under wet conditions.

Also shown in Figure 13 are three models for which D_c has different depth variations at shallower depths. For model B, D_c is assumed to be constant regardless of depth. This depth-independence of D_c is what has been presumed in earlier papers (e.g., Dieterich, 1978; Tse and Rice, 1986).

In the remaining two models, D_c either increases (model A) or decreases (model C) with depth. At very shallow depths, D_c may decrease with increasing depth because of the stabilizing effect due to unconsolidated gouge materials with which well-developed fault zones at about 2–4 km depths are likely to be filled (Marone and Scholz, 1988). Such stabilizing effect has been incorporated into model A.

3.3. *Breakdown stress drop*

It has been found for initially intact Westerly granite that $\Delta\tau_b/\sigma_n$ decreases with increasing temperature above 300°C, below which $\Delta\tau_b/\sigma_n$ may be considered roughly constant. However, this result is not directly applicable for estimating the breakdown stress drop at a shallow part of the lithosphere, because the magnitude of $\Delta\tau_b$ at shallow crustal depths may be governed by frictional behaviour on preexisting faults. The frictional sliding process is either of a stable or unstable mode. The stability of frictional sliding is controlled by a variety of factors such as normal stress across the fault, temperature, pore pressure, porosity, gouge layer thickness, and roughness of sliding surfaces (e.g., Brace and Byerlee, 1966; Brace, 1972). Although the stability is also influenced by rock type, granitic lithosphere has been assumed in the present paper. Among the above influencing factors, the effects of effective normal stress and temperature are primarily important, and earlier experiments (e.g., see Brace, 1972) show that the high normal stress and low temperature destabilize frictional sliding. The stability analysis of frictional sliding (Ruina, 1983; Rice and Ruina, 1983) shows that frictional stability or instability is determined by the sign of the friction property $d\tau^{ss}/dV$, where τ^{ss} is the steady-state frictional resistance, and V is the slip velocity; that is, if $d\tau^{ss}/dV < 0$, steady-state frictional sliding is unstable in a system of sufficiently low stiffness or in a stiff system subjected to sufficiently strong perturbations from the steady state, and otherwise sliding is stable when $d\tau^{ss}/dV > 0$. The stability of frictional sliding can also be determined by whether or not the rate of decrease in shear resistance with slip is slower than the rate of elastic unloading of the surrounding system (e.g., Tse and Rice, 1986), and the depth variation of the breakdown stress drop as well as the critical slip displacement is crucial for discussing the nucleation of stick-slip shear instability and the shallow depth confinement of seismicity. We here roughly estimate on the basis of available experimental data how the magnitude of the breakdown stress drop, affected by pressure and temperature, varies with depth.

Brace and Byerlee (1970) and Stesky et al. (1974) found that the transition from stable to unstable frictional slip occurs at about 300°C. Stesky (1978) further found for dry Westerly granite that the velocity-dependence of friction was positive in the temperature range 300°–700°C, while Lockner et al. (1986) found for dry Westerly granite gouge that the velocity-dependence was zero to slightly positive over the range 23°–850°C, with isolated stick-slip events below 300°C.

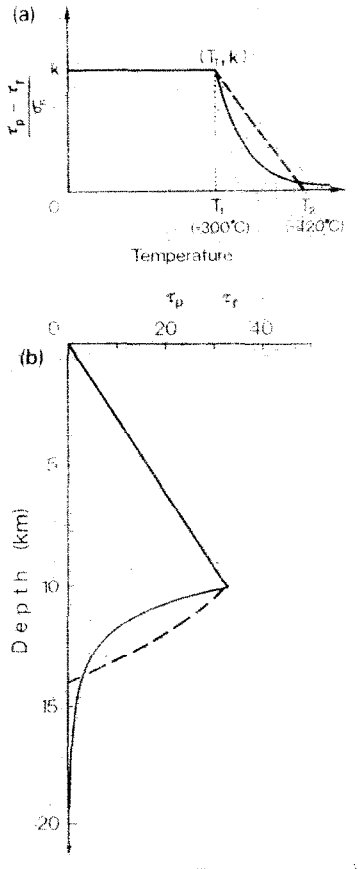

Fig. 14. (a) A rough estimate of the relation between $\Delta\tau_b/\sigma_n$ and temperature, and (b) the resulting depth variation of $\Delta\tau_b$ for a given geothermal gradient (30°C/km).

Recent observation for wet Westerly granite gouge by Blanpied et al. (1991) showed the velocity-weakening in the range 100°–350°C, and the velocity-strengthening over the range 350°–600°C. With these observations in mind, we assume that the magnitude of $\Delta\tau_b/\sigma_n$ for stick-slip decreases transitionally to zero in a range from 300°C to a higher temperature. This will be a reasonable assumption, because $\Delta\tau_b/\sigma_n$ should diminish with increasing temperature. It is difficult to assess the critical temperature above which $\Delta\tau_b/\sigma_n$ becomes negligibly small or vanishes. In Figure 8, the temperature above which $\Delta\tau_b/\sigma_n$ becomes negligibly small is found to be about 900°K (= 627°C). This indicates that the critical temperature is about 630°C for initially intact dry Westerly granite, which may give a possible highest value for the critical temperature in a dry environment. Plasticity should, at least partly, be responsible for the critical temperature, so that the critical temperature will be reduced significantly in wet environments. As an example, we illustrate in Figure 14 the case in which $\Delta\tau_b/\sigma_n$ becomes negligibly small above 420°C. This value for the critical temperature does not overly differ from that inferred from friction experiments. In the stability analysis of frictional sliding, the following parameters defined by:

$$a = V(\partial\tau/\partial V)_{\text{instantaneous}}$$
$$a - b = V\,\mathrm{d}\tau^{ss}/\mathrm{d}V \qquad (14)$$

are often used, and the parameter b here has a physical meaning similar to $\Delta\tau_b$. Tse and Rice (1986), using Stesky's (1975) experimental data, estimated b to be about 407°C, so that the case shown in Figure 14 may not be an unreasonable example.

Since Westerly granite below 300°C is in the brittle regime, $\Delta\tau_b$ for stick-slip is normal stress-dependent but temperature-insensitive below 300°C. It has been established that $\Delta\tau_b$ for stick-slip is proportional to the normal stress acting on the fault. The magnitude of the proportionality constant k ($= \Delta\tau_b/\sigma_n$) depends on a variety of factors, but such detailed discussion is not necessary for the present purpose. As an example, we take the case of $k = 0.3$ below 300°C, above which $\Delta\tau_b/\sigma_n$ gradually decreases to zero with increasing temperature, as shown in Figure 14a. In general, the fracture energy must be finite in the transition zone from unstable to stable slip, and as the simplest case, it is assumed here that the fracture energy is maintained constant in this transition zone. Under this assumption, $\Delta\tau_b/\sigma_n$ decreases exponentially with temperature if D_c increases with temperature according to an equation of the form of eq. 11, or $\Delta\tau_b/\sigma_n$ decreases linearly with temperature if D_c increases with temperature according to an equation of the form of eq. 12. In this treatment, the steady-state frictional sliding is regarded as a limiting case of $\Delta\tau_b \to 0$ and $D_c \to \infty$. These two cases are shown in Figure 14a as examples, on the basis of which the variation of $\Delta\tau_b$ at crustal depths is depicted in Figure 14b.

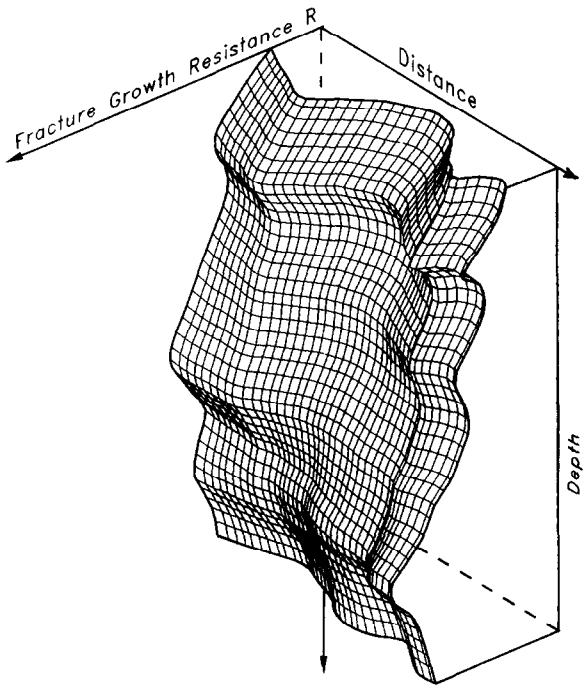

Fig. 15. A schematic example of spatial local variation of rupture growth resistance.

We have to bear in mind that depth variations of τ_{tect}, D_c and $\Delta\tau_b$ estimated above show only general trends. In reality, as discussed in the beginning of this section, short-wavelength variations that will exist on a local scale would be superimposed, as illustrated in Figure 15. Using depth variations of these estimated parameters

makes it possible to computer-simulate the earthquake rupture nucleation in the lithosphere. One attempt of such simulation has been made in a separate paper (Yamashita and Ohnaka, 1992). Depth profile of the shear resistance, such as shown in Figures 5 and 6, has been compared with depth confinement of seismicity (Sibson, 1982, 1984); however, it may also be interesting to compare depth profiles of D_c and $\Delta\tau_b$ shown in Figures 13 and 14 with depth confinement of seismicity as shown in Figure 20.

4. Earthquake nucleation and immediate foreshocks

As discussed in Section 2, whether or not the earthquake rupture is preceded by foreshock activity during the quasistatic nucleation, leading to quasidynamic one at a later time, depends on how inhomogeneously the rupture growth resistance prevails in the fault zone. Immediate foreshocks have been defined in this paper as local dynamic instabilities that occur in the process of the quasistatic to quasidynamic nucleation of the ensuing overall dynamic instability. Jones and Molner (1979) and Scholz (1988a) pointed out that typical immediate foreshocks that are concentrated close to its hypocentral region, begin to appear less than about 10 days before the mainshock. This empirical fact may give a suggestion for the time window to identify immediate foreshocks, and we here employ a 10-day period as the time window. A specific size for the space window to be used to identify such immediate foreshocks may be difficult to generalize, because it should differ according to the nucleation zone size of individual earthquake mainshocks, which in turn depends on spatial distribution of rupture growth resistance resulting, for instance, from geologic or geostructural setting of the fault zone. As we have discussed in Section 2, the entire process of earthquake nucleation can include local dynamic instabilities. In this case, the average rupture growth rate during the nucleation will be much higher than the completely stable, quasistatic rupture growth rate caused by the accumulation of tectonic stress. If the average rupture growth rate during the nucleation is assumed to be of the order of 0.01 m/s, and if quasistatic to quasidynamic rupture during the nucleation spreads bi-directionally, then the nucleation zone extends to the size of 17.3 km in the 10-day period. This may give a suggestion for the space window to identify immediate foreshocks. We here discuss the following two cases that may particularly be interesting from a tectonic viewpoint: (1) interplate earthquakes at a transform fault boundary that nucleate below the base of the brittle seismogenic layer, and (2) intraplate earthquakes that nucleate within the brittle seismogenic layer.

4.1. Nucleation below the base of the brittle seismogenic layer

At a transform fault boundary, slip occurs intermittently by seismic faulting at shallow crustal depth, while aseismic slip or continuous shear deformation is expected to occur at greater depth, driven by horizontal steady-flow motion in the lower crustal asthenosphere (Savage and Burford, 1973; Turcotte and Spence, 1974; Li and Rice, 1983a). In the interseismic period, the fault is locked within the seismogenic depth, while aseismic slip occurs below the locked part of the fault zone. Thus, elastic shear deformation accumulates in the vicinity of the locked part of the fault (Savage and Burford, 1973; Turcotte and Spence, 1974; Li and Rice, 1983a). In such a situation at the transform plate boundary, the depth variation of the rupture growth resistance, in particular that of the critical slip displacement in the transition layer from the brittle to plastic regime, is important in simulating the earthquake nucleation.

A mathematical analysis using a realistic model into which depth variation of the rupture growth resistance is incorporated (Yamashita and Ohnaka, 1992) shows that if the parameter AD_{co} in eq. 11 is assumed to be small, rupture begins to nucleate stably and quasistatically far below the base of the seismogenic layer, and the tip of the stable and quasistatic nucleation zone progresses upward unidirectionally according to a constant build-up of tectonic stress, as has been discussed by earlier authors (Dmowska and Li, 1982; Li and Rice, 1983b). This stable and quasistatic upward

progression of the tip of the nucleation zone develops into dynamic instability giving rise to overall seismic rupture of the locked part of the fault zone, shortly after the tip of the nucleation zone has penetrated through an asperity patch of the strongest rupture growth resistance near the base of the seismogenic layer (Yamashita and Ohnaka, 1992). Since the nucleation below the base of the seismogenic layer proceeds necessarily aseismically, foreshocks are not expected to occur during this nucleation process. The mathematical analysis (Yamashita and Ohnaka, 1992) further shows that earthquake dynamic instability can suddenly occur near the base of the seismogenic layer without full development of the stable and quasistatic nucleation, if the critical slip displacement is large enough. This means that earthquake rupture suddenly occurs without any immediate foreshocks. Thus, carrying no conspicuous immediate foreshock activity would be a common characteristic of large earthquakes that begin to rupture dynamically near the base of the brittle seismogenic layer at the transform plate boundary. A typical example for this is the 1989 Loma Prieta earthquake (M_s 7.1). The Loma Prieta earthquake occurred at 17h04 (p.d.t.) on 17 October 1989 in the San Francisco Bay area; its hypocentre was located at a depth of 17.6 km on the San Andreas transform fault, and the rupture spread unidirectionally upward and bilaterally along strike, with nearly equal components of right-lateral strike-slip and reverse slip (U.S. Geological Survey Staff, 1990). This earthquake carried no obvious short-term seismic precursors (U.S. Geological Survey Staff, 1990). One may argue that the 27 June 1988 (M 5.0) and 8 August 1989 (M 5.2) Lake Elsman earthquakes (see Note 16 of U.S. Geological Survey Staff, 1990) were foreshocks of the Loma Prieta earthquake. This may be so, but these earthquakes may not be regarded as immediate foreshocks that occur in the nucleation zone, since they occurred more than two months prior to the mainshock.

4.2. Nucleation within the brittle seismogenic layer

For an earthquake that nucleates within the brittle seismogenic layer, inhomogeneous spatial distribution of the rupture growth resistance on a local to small scale within the layer is of primary concern. In this case, inhomogeneous distribution of the rupture growth resistance on a local to small scale may be prescribed by geological and geometrical (or topographical) settings of the fault zone (or fault surfaces), and local fluctuation of pore water pressure (temperature-insensitive in the brittle regime). As noted in the foregoing section, fault surfaces within the brittle seismogenic layer have fractal roughnesses of a bounded wavelength band (e.g., Aviles et al., 1987; Okubo and Aki, 1987). The nucleation process in this situation is greatly influenced by the existence of "asperities" or "barriers" on the fault that are local patches of greater rupture growth resistance. These patches may be products resulting from such geological and geometrical settings in the fault zone, and/or from local fluctuations of pore water pressure. Since those patches are considered to prevail on a local to small scale in the fault zone in the brittle seismogenic layer, carrying immediate foreshocks will be one of the major characteristics of earthquakes that nucleate within the brittle seismogenic layer. Immediate foreshock activity is a part of the nucleation process leading to the mainshock rupture (Section 2), so that hypocentral locations of these foreshocks are necessarily restricted to lie near the mainshock hypocentre.

As we have discussed in Section 2, the question of where an earthquake rupture nucleates, depends on the depth distribution of parameters such as the shear resistance, the breakdown stress drop and the critical slip displacement. For instance, if we assume (1) that overall depth distribution of shear resistance is represented by the curves shown in Figure 6, (2) that overall depth distribution of the critical slip displacement at depths shallower than 10 km is given by curve A in Figure 13, and (3) that overall depth distribution of the breakdown stress drop is represented by the curve shown in Figure 14b, then the plausible depth at which an earthquake rupture begins to nucleate is likely to be at 3–4 km or shallower (much shallower than the base of the seismogenic layer), since the rupture growth resistance can be at a minimum there if the short

wavelength variations that will exist on a local scale are superimposed on the general trend (see Fig. 15). The nucleation of intraplate earthquakes that will be discussed below may be regarded as such a case.

First let us consider the case where both tips of the zone of the nucleation that has occurred at a shallow depth in the brittle seismogenic layer, progress bi-directionally downward and upward along paths of minimum resistances for rupture growth within the brittle seismogenic layer (for a conceptual model of this case see Fig. 16). In this case, the depth variation of the rupture growth resistance (such as illustrated in Fig. 15) is of primary concern, and the earthquake instability resulting in overall rupture of the fault within the brittle seismogenic layer can occur (M in Fig. 16) after the progressing tip of the nucleation zone has penetrated through a local asperity patch of the largest rupture growth resistance, which is anticipated to exist near the base of the seismogenic layer. Foreshock activity (F_1, F_2, ..., in Fig. 16), which can occur during this nucleation when the rupture growth resistance varies on a local to small scale, should necessarily be restricted to lie within a localized region shallower than the hypocentre depth of the mainshock located near the base of the seismogenic layer. Such a typical example is the Mikawa earthquake (M_{JMA} 6.8), which occurred at 03h38 on 13 January 1945 in the Mikawa Bay, 50 km to the south of Nagoya City, central Japan (Hamada, 1986, 1987).

Hamada (1986, 1987) has carefully reexamined and relocated the hypocentres of foreshocks, mainshock and aftershocks for the Mikawa earthquake. Ten foreshocks are listed in his catalog (Hamada, 1986), and these foreshocks began to occur 6 days before the mainshock took place, but most foreshocks were concentrated in the period of 41–27 hours prior to the mainshock. Since no foreshocks listed in Hamada's catalog took place during the period of about 27 h before the mainshock, a lull in foreshock activity is likely to have occurred immediately before the Mikawa earthquake. For eight of the ten foreshocks listed, the magnitudes are determined, which range from 4.1 to 5.7. Figure 17 shows epicentral locations of immediate foreshocks (dots), which were concentrated in the vicinity of the epicentre of the mainshock (star) for the Mikawa earthquake. Its aftershocks were roughly located in the shaded area in Figure 17 (Hamada, 1986, 1987). Since most aftershocks of the Mikawa earthquake have been located at depths shallower than 14 km (Hamada, 1986, 1987), the mainshock hypocentre is considered to be near the base of the seismo-

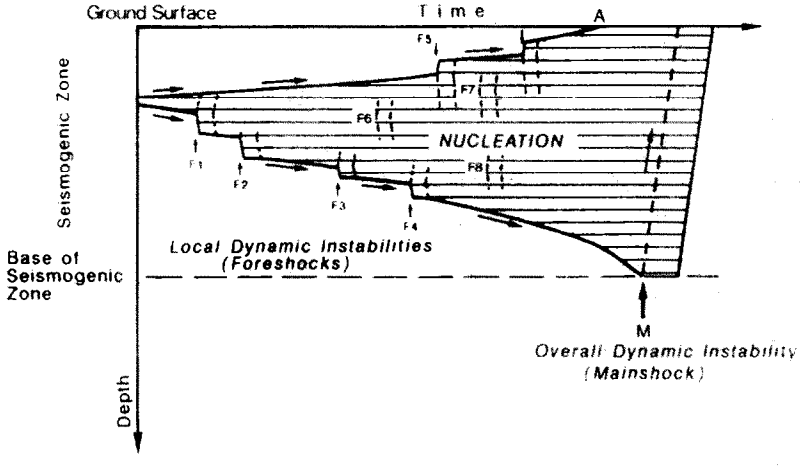

Fig. 16. A conceptual model for earthquake rupture nucleation that progresses bi-directionally upward and downward. The shaded portion denotes the breakdown zone. F_1, F_2, etc., represent the occurrence of local dynamic instabilities (foreshocks), and M denotes the occurrence of overall dynamic instability (mainshock). Note that local dynamic instabilities can occur within the nucleation zone. The point A indicates where the earthquake fault breaks out to the earth's surface; however, in reality, some faults may not break out to the surface.

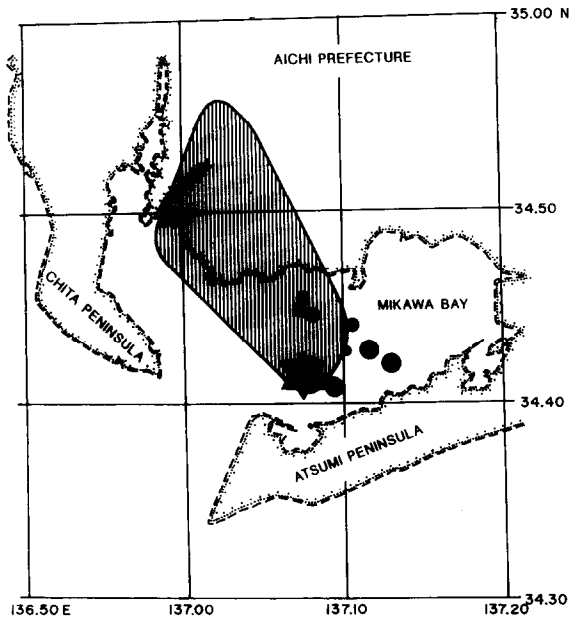

Fig. 17. Epicentral locations of foreshocks and mainshock for the 1945 Mikawa earthquake. Dots and star indicate foreshocks and mainshock, respectively. Aftershocks were located in the shaded portion. Data from Hamada (1986).

genic layer. The seismicity confinement of within 14 km depth in this region is compatible with depth profiles of the shear resistance, the breakdown stress drop and the critical slip displacement in a wet environment (see Figs. 6, 13 and 14b), if the temperature gradient in this particular region is considered to be lower than 30°C/km. The depth distribution of the hypocentres of these foreshocks and mainshock is shown in Figure 18. The shaded portion in Figure 18 indicates the fault area of the mainshock roughly inferred from the aftershock distribution. Hamada (1987) has found that the hypocentral depths of foreshocks relocated are all shallower than that of the mainshock relocated at a depth of 12.4 km. This is an important feature, and this feature is what is expected from the present model (Fig. 16).

In the case where the rupture growth resistance is larger in the upward and downward directions than in the lateral directions, the nucleation has no alternative but to proceed along fault strike. In such a case, horizontal local variation of the rupture growth resistance along strike is of main concern. Since lithostatic pressure is considered constant at the same crustal depth, horizontal local distribution of the rupture growth resistance would be determined primarily by geological and geometrical local to small structures of the fault zone, and/or local fluctuation of pore water pressure. A typical example for this case is the 1978 Izu Oshima Kinkai earthquake (M_{JMA} 7.0), which occurred in the area of Izu Oshima Island and the Izu Peninsula, Japan, at 12h25 on 14 January 1978. This earthquake has been known for its conspicuous immediate foreshock activity (Tsumura et al., 1978). Nevertheless, a series of foreshock activity for the 1978 Izu Oshima Kinkai earthquake has not fully been analyzed, and it will be discussed rather in detail below.

The earthquake catalog *List of Earthquakes in the Kanto Area and its Vicinity*, compiled by Matsu'ura et al. (1988) and published by the Earthquake Research Institute, makes it possible to examine a series of nucleation processes for the Izu Oshima Kinkai earthquake. From this catalog, we selected earthquakes of $M \geqslant 2.0$ of

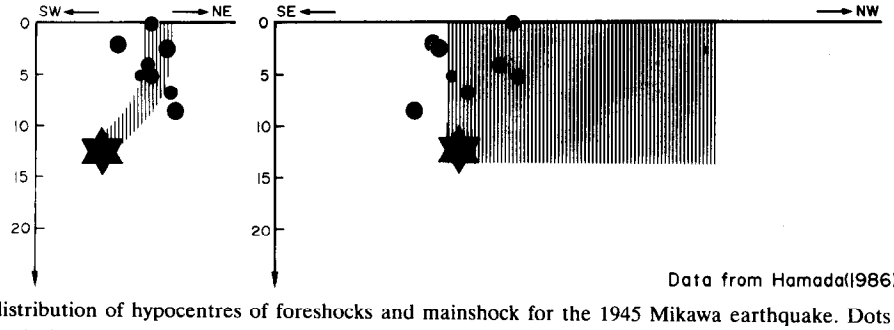

Fig. 18. Depth distribution of hypocentres of foreshocks and mainshock for the 1945 Mikawa earthquake. Dots and star indicate foreshocks and mainshock, respectively. The shaded portion indicates the fault area of the mainshock roughly inferred from the aftershock distribution.

which the hypocentres had been determined from the data at six or more than six stations, and these selected data alone have been used for the present analysis, since they may be regarded as most reliable. According to these data, immediate foreshocks of $M \geq 2.0$ for the Izu Oshima Kinkai

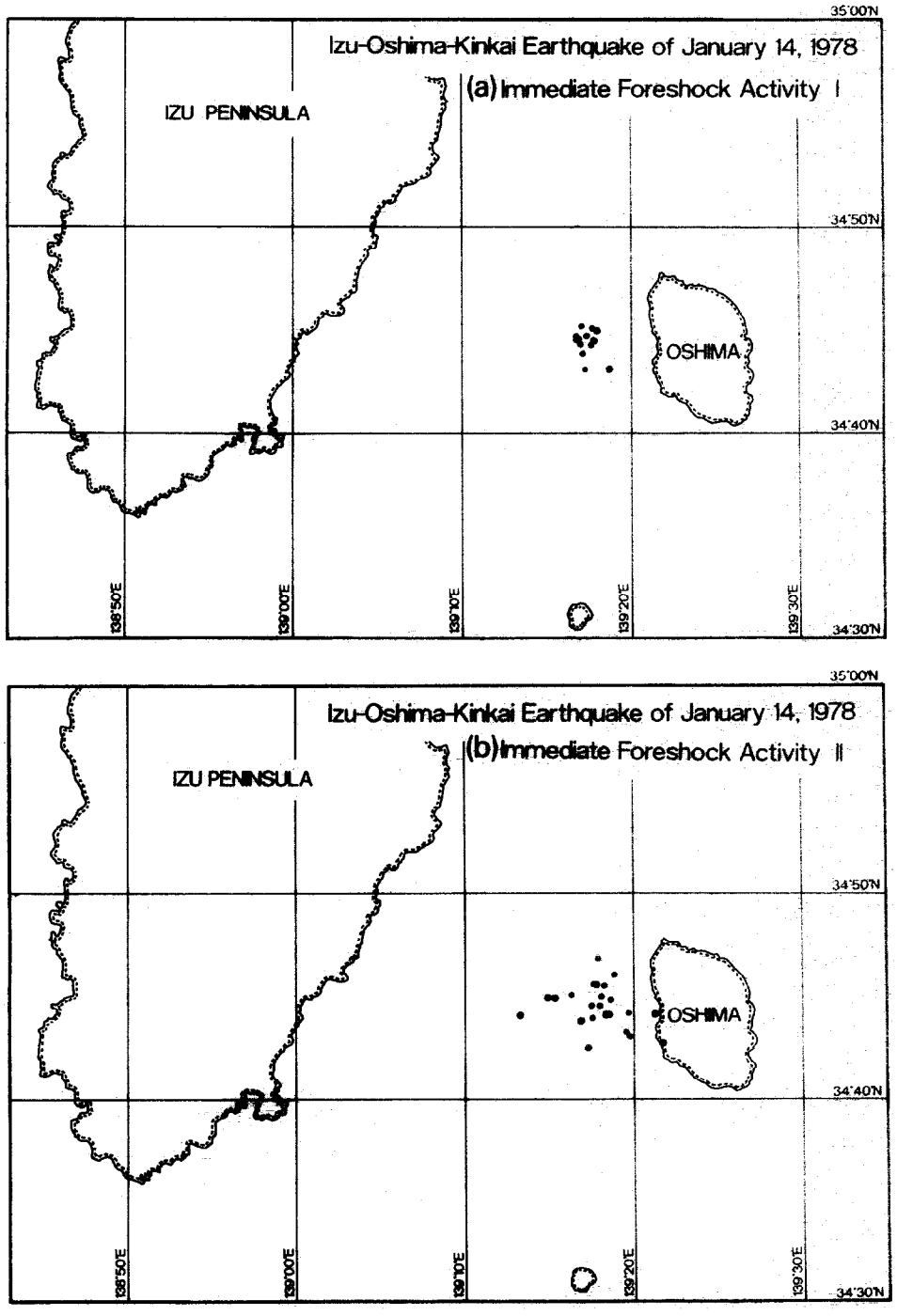

Fig. 19. Epicentral locations of foreshocks, mainshock, and aftershocks ($M \geq 2.0$) for the 1978 Izu Oshima Kinkai earthquake: (a) foreshocks at phase I; (b) foreshocks at phase II; (c) foreshocks at phase III and mainshock (star); and (d) aftershocks. The arrow in (c) indicates the direction of the mainshock rupture. The thick line in (d) denotes the mainshock fault strike inferred (Shimazaki and Somerville, 1979; Kikuchi and Sudo, 1984). Data from the Earthquake Catalog by Matsu'ura et al. (1988).

earthquake began to occur at about 17h40 on 13 January 1978 in an area near the hypocentre of the ensuing mainshock. The entire period from this time to the time of the mainshock occurrence may tentatively be divided into three phases: phase I (15 h and 20 min from 17h40 on 13 January) in which foreshocks were concentrated within a very small limited area; phase II (1 h and 10 min) in which foreshocks began to migrate toward its environs; and phase III (2 h and 14

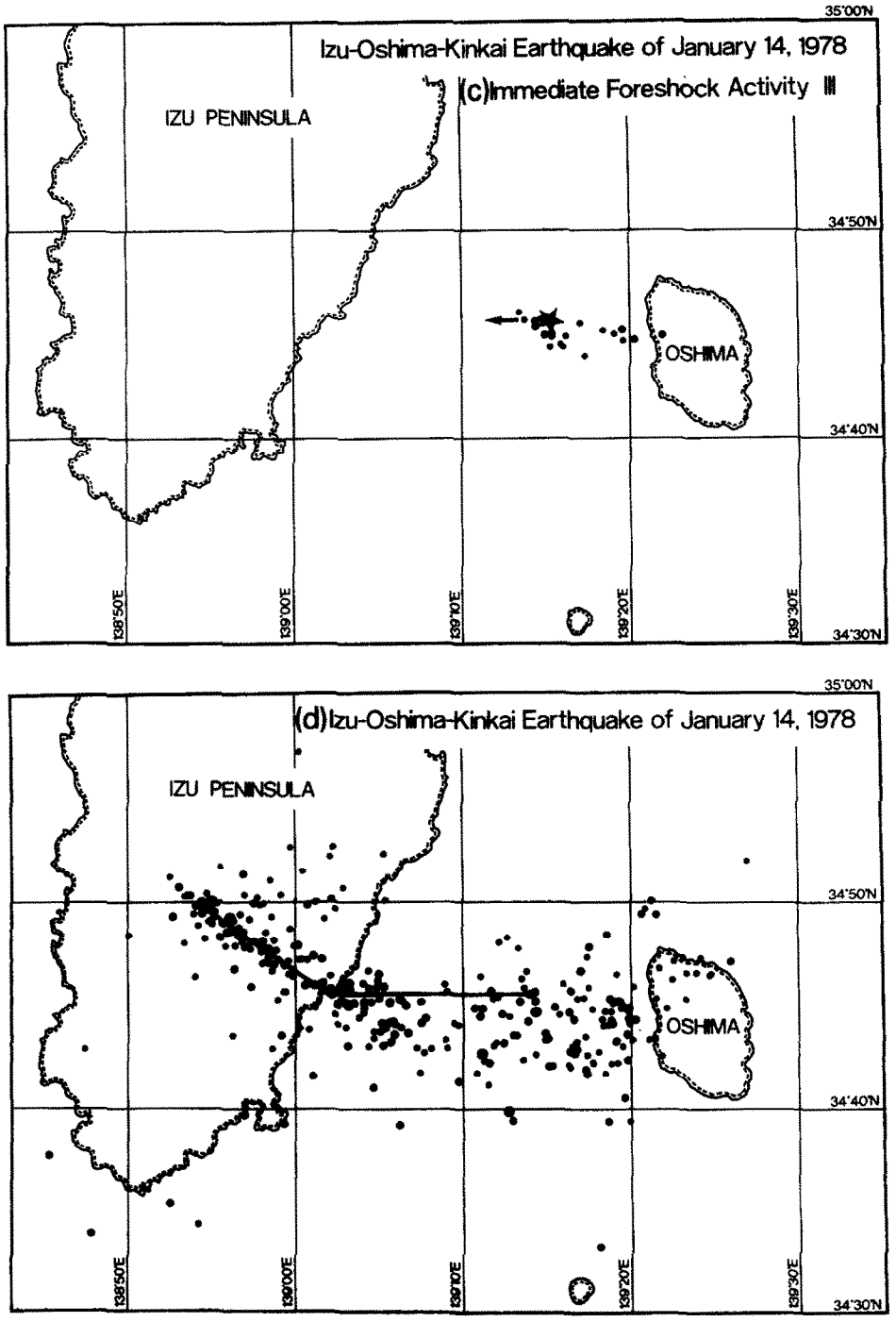

Fig. 19. (continued)

min) in which foreshocks continued to migrate along strike until the mainshock took place. Phase I may be regarded as the initial stage of immediate foreshock activity, and phase III as the final stage. The two largest foreshocks of M 5.1 took place successively during phase II. Epicentral locations of these immediate foreshocks of $M \geq 2$ for the Izu Oshima Kinkai earthquake at individual phases are shown in Figures 19a–19c. Figures 20a–20c show the depth distributions of the hypocentres for these foreshocks at the same phases. The star in Figures 19c and 20c denotes the mainshock hypocentre, which was located at a depth of 4 km, about 10 km west of Izu Oshima Island. Hypocentral locations of aftershocks with $M \geq 2.0$ are also shown in Figures 19d and 20d for reference. The mainshock rupture, its foreshock and aftershock activities were restricted to within 10 km depth. This suggests that the base of the seismogenic layer in this particular region is

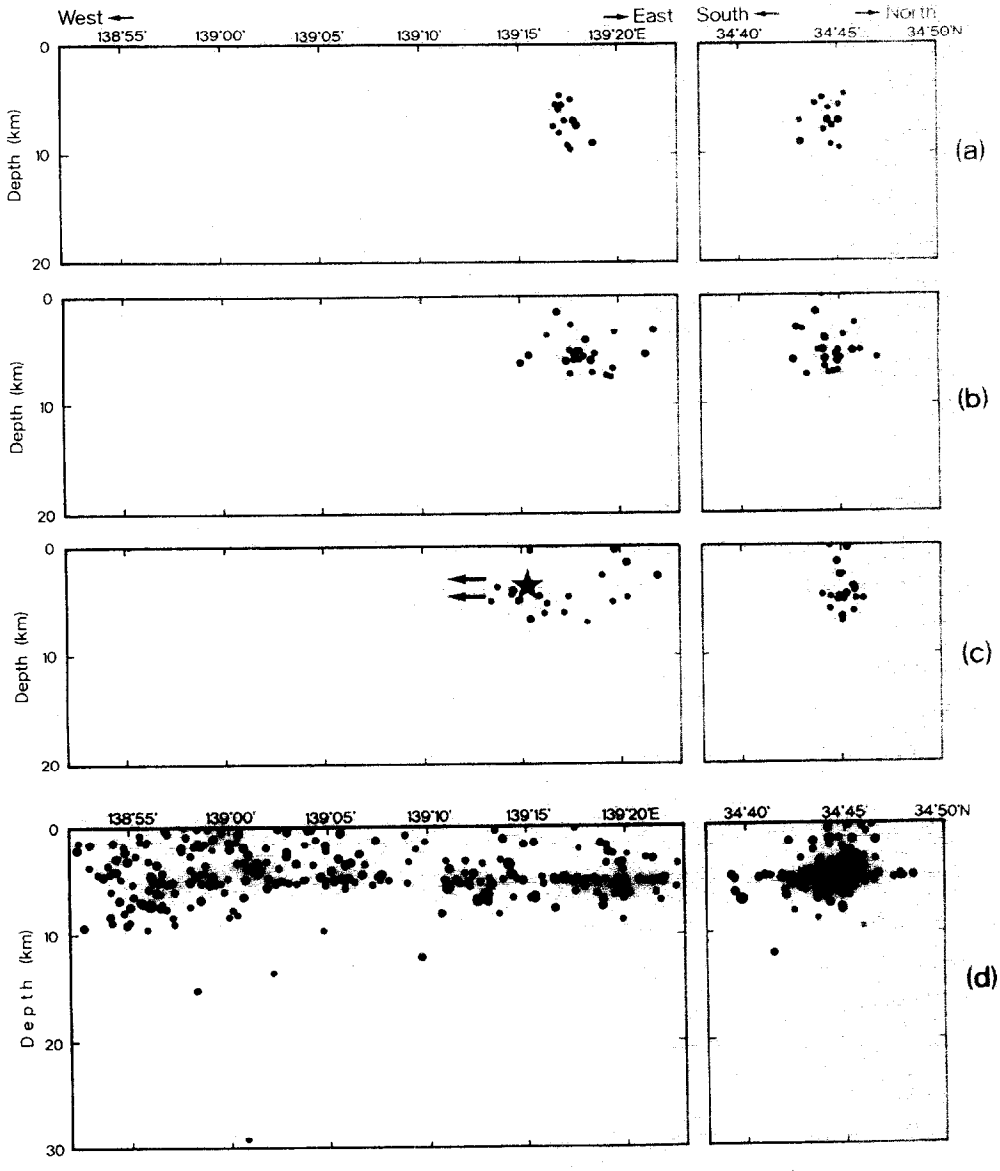

Fig. 20. Depth distribution of hypocentres of foreshocks, mainshock, and aftershocks ($M \geq 2.0$) for the 1978 Izu Oshima Kinkai earthquake: (a) foreshocks at phase I; (b) foreshocks at phase II; (c) foreshocks at phase III and mainshock (star); and (d) aftershocks. The arrows in (c) indicate the direction of the mainshock rupture. Data from the Earthquake Catalog by Matsu'ura et al. (1988).

at a depth of 10 km, which is compatible with depth profiles of the shear resistance, the critical slip displacement and the breakdown stress drop in a wet environment, shown in Figures 6, 13 and 14b.

As discussed in Section 2, the present model suggests that the mainshock nucleation occurred in the zone that includes the region where foreshocks began to concentrate; in other words, the region where immediate foreshocks were concentrated is a part of the zone of the mainshock nucleation. The migration of foreshock activity may mean that the nucleation zone developed with time. It is found from Figures 19 and 20 that a lull in foreshock activity occurred at phase III in the small area where it had been active in the initial stage (phase I). The area where the lull in foreshock activity occurred in phase III may be the zone where the stress had decreased to a residual friction stress level (Section 2). Development of the nucleation zone eventually leads to the mainshock dynamic rupture, which began to propagate westward unilaterally at the hypocentre (star mark in Figs. 19 and 20) (Shimazaki and Somerville, 1979; Kikuchi and Sudo, 1984). Why did the mainshock rupture propagate westward unilaterally? This would be because the rupture growth resistance is weaker in the western part of the locked fault, and/or because the elastic strain energy to be released is less stored in its eastern part, so that the rupture has no alternative but to propagate westward (note that Oshima Island is an active volcano). Since the mainshock nucleation proceeds in a zone that includes the hypocentral region of immediate foreshocks, preseismic slip and premonitory stress change would have been observed in (or near) the particular area where immediate foreshocks occurred, if the monitoring instruments had been suitably installed.

5. Conclusion

Earthquake instability giving rise to dynamically propagating rupture over the entire fault is locally preceded by stable (or pseudo-stable), quasistatic to quasidynamic nucleation processes even in the purely brittle regime, if the rupture growth resistance is nonuniformly distributed on the fault (Ohnaka and Kuwahara, 1990; Yamashita and Ohnaka, 1991). Whether or not a sizable zone of stable (or pseudo-stable), quasistatic to quasidynamic nucleation appears prior to the earthquake dynamic instability depends on how the rupture growth resistance prevails nonuniformly in the fault zone in the lithosphere. This nucleation process is an intrinsic part of the ensuing unstable dynamic rupture; in other words, the nucleation process itself is an earthquake precursor that occurs in a localized zone. Hence, the key to a short-term earthquake prediction is to identify where the nucleation occurs on the fault that has the potential to cause a major earthquake. During the earthquake nucleation, local shear stress decreases gradually in the breakdown zone, and at the same time the corresponding premonitory slip also proceeds in the zone, since slip-weakening occurs during the nucleation. Premonitory stress (or strain) changes can also be expected to occur outside (but adjacent to) the nucleation zone. Immediate foreshock activity is a part of the nucleation process leading to the mainshock rupture; therefore, hypocentral locations of foreshocks are necessarily restricted to lie near the mainshock hypocentre. Whether or not foreshocks occur during the mainshock nucleation depends on how the rupture growth resistance varies on a local to small scale. Variation of the rupture growth resistance on a local to small scale would result from geological and geometrical (or topographical) settings in the fault zone (or its surfaces), and/or local fluctuation of pore water pressure. Patches of higher effective breakdown stress have greater critical slip displacement (Figs. 10 and 11). A lull in foreshock activity just before the mainshock is expected when local stresses have decreased to a residual friction stress level in most parts of the nucleation zone.

Overall depth variation of the rupture growth resistance in the lithosphere results primarily from the nonuniform distribution of ambient pressure and temperature at crustal depths. To estimate depth variations of the parameters τ_p, $\Delta\tau_b$, and D_c, which are indicative of the rupture growth resistance, the combined effects of pressure and

temperature have been investigated by using the available laboratory data so far published. The effect of temperature on τ_p in the semibrittle regime can be represented by eq. 3. D_c increases sharply with temperature but is insensitive to normal stress above 300°C, while it depends on normal stress but is insensitive to temperature below 300°C. Although the temperature effect on D_c is difficult to assess uniquely because of the limited number of available data, it can be represented by eq. 11 or 12. D_c is indicative of the stabilizing effect of slip failure. On the basis of these results, variation in the shear resistance, the breakdown stress drop and the critical slip displacement at mid-crustal depths has been estimated for granite for a given geothermal gradient. The shear resistance does not have a sharp peak at mid-crustal depths. The critical slip displacement increases with depth at mid-crustal depths.

Since the nucleation process below the base of the seismogenic layer is aseismic in nature, carrying no conspicuous foreshock activity will be a common characteristic of interplate earthquakes that nucleate below the base of the brittle seismogenic layer. A typical example for this case is the 1989 Loma Prieta earthquake. Since patches of greater rupture growth resistance are considered to prevail on a local to small scale in the fault zone in the brittle seismogenic layer, carrying immediate foreshocks will be one of the major characteristics of earthquakes that nucleate within the brittle seismogenic layer. The 1978 Izu Oshima Kinkai earthquake is a typical example for this case. When a mainshock earthquake nucleates quasistatically or quasidynamically at a shallow depth within the brittle seismogenic layer, and when its overall dynamic rupture occurs near the base of the seismogenic layer, its immediate foreshocks expected are necessarily restricted to lie within a localized region shallower than the hypocentral depth of the mainshock. A typical example is the 1945 Mikawa earthquake.

Acknowledgements

Experimental data from Griggs et al., Stesky et al., and Wong were valuable in the present study, and I thank them for having published their data. I am grateful to T.-F. Wong for supplying a reprint of his study. I am also grateful to N. Hamada for providing a copy of his Doctor thesis and materials for the 1945 Mikawa earthquake, and K. Abe for discussions on the 1989 Loma Prieta earthquake. Critical comments by anonymous reviewers were helpful in revising the original manuscript, for which I am grateful. This research was supported in part by a grant from the Ministry of Education, Science and Culture of Japan (project number 63460039).

References

Atkinson, B.K. (Editor), 1987. Fracture Mechanics of Rock. Academic Press, London, 534 pp.

Aviles, C.A., Scholz, C.H. and Boatwright, J., 1987. Fractal analysis applied to characteristic segments of the San Andreas fault. J. Geophys. Res., 92: 331–344.

Blacic, J.D., 1975. Plastic-deformation mechanisms in quartz: The effect of water. Tectonophysics, 27: 271–294.

Blanpied, M.L., Lockner, D.A. and Byerlee, J.D., 1991. Fault stability inferred from granite sliding experiments at hydrothermal conditions. Geophys. Res. Lett., 18: 609–612.

Bodri, B., Iizuka, S. and Hayakawa, M., 1989. Modeling of deep temperatures and heat flow in central Honshu, Japan. J. Geodyn., 11: 105–129.

Brace, W.F., 1972. Laboratory studies of stick-slip and their application to earthquakes. Tectonophysics, 14: 189–200.

Brace, W.F. and Byerlee, J.D., 1966. Stick-slip as a mechanism for earthquakes. Science, 153: 990–992.

Brace, W.F. and Byerlee, J.D., 1970. California earthquakes: Why only shallow focus? Science, 168: 1573–1575.

Brown, S.R. and Scholz, C.H., 1985. Broad bandwidth study of the topography of natural rock surfaces. J. Geophys. Res., 90: 12575–12582.

Byerlee, J.D., 1978. Friction of rocks. Pure Appl. Geophys., 116: 615–626.

Carter, N.L., 1976. Steady state flow of rocks. Rev. Geophys. Space Phys., 14: 301–360.

Carter, N. and Kirby, S.H., 1978. Transient creep and semibrittle behavior of crystalline rocks. Pure Appl. Geophys., 116: 807–839.

Dieterich, J.H., 1978. Time-dependent friction and the mechanics of stick-slip. Pure Appl. Geophys., 116: 790–806.

Dmowska, R. and Li, V.C., 1982. A mechanical model of precursory source processes for some large earthquakes. Geophys. Res. Lett., 9: 393–396.

Eaton, J.P., Lee, W.H.K. and Pakiser, L.C., 1970. Use of microearthquakes in the study of the mechanics of earthquake generation along the San Andreas fault in central California. Tectonophysics, 9: 259–282.

Griggs, D., 1967. Hydrolytic weakening of quartz and other silicates. Geophys. J.R. Astron. Soc., 14: 19–31.

Griggs, D.T. and Blacic, J.D., 1965. Quartz: anomalous weakness of synthetic crystals. Science, 147: 292–295.

Griggs, D.T., Turner, F.J. and Heard, H.C., 1960. Deformation of rocks at 500° to 800°C. In: D. Griggs and J. Handin (Editors), Rock Deformation. Geol. Soc. Am., Mem., 79: 39–104.

Hamada, N., 1986. Re-Examination of Seismicity Associated with Destructive Inland Earthquakes of Japan and Its Seismological Significance. Dr. Thesis, Univ. Tokyo, 175 pp.

Hamada, N., 1987. Re-examination of seismicity associated with destructive inland earthquakes of Japan and its seismological significance. Pap. Meteorol. Geophys., 38: 77–156.

Hansen, F.D. and Carter, N.L., 1982. Creep of selected crustal rocks at 1000 MPa. EOS, AGU, 63: 437.

Jaeger, J.C. and Cook, N.G.W., 1976. Fundamentals of Rock Mechanics (2nd ed.). Chapman and Hall, London, 585 pp.

Jones, L.M. and Molnar, P., 1979. Some characteristics of foreshocks and their possible relationship to earthquake prediction and premonitory slip on faults. J. Geophys. Res., 84: 3596–3608.

Kekulawala, K.R.S.S., Paterson, M.S. and Boland, J.N., 1978. Hydrolytic weakening in quartz. Tectonophysics, 46: T1–T6.

Kikuchi, M. and Sudo, K., 1984. Inversion of teleseismic P waves of Izu–Oshima, Japan earthquake of January 14, 1978. J. Phys. Earth, 32: 161–171.

Kuwahara, Y., Ohnaka, M., Yamamoto, K. and Hirasawa, T., 1985. Effects of the fault surface roughness on unstable slip and a scaling law of slip. Annu. Mtg. Seismol. Soc. Jpn., Progr. Abstr., 2: 110.

Kuwahara, Y., Ohnaka, M., Yamamoto, K. and Hirasawa, T., 1986. Accelerating process of rupture during stick-slip failure. Annu. Mtg. Seismol. Soc. Jpn., Progr. Abstr., 2: 233.

Li, V.C. and Rice, J.R., 1983a. Preseismic rupture progression and great earthquake instabilities at plate boundaries. J. Geophys. Res., 88: 4231–4246.

Li, V.C. and Rice, J.R., 1983b. Precursory surface deformation in great plate boundary earthquake sequences. Bull. Seismol. Soc. Am., 73: 1415–1434.

Lockner, D.A., Summers, R. and Byerlee, J.D., 1986. Effects of temperature and sliding rate on frictional strength of granite. PAGEOPH, 124: 445–469.

Marone, C. and Scholz, C.H., 1988. The depth of seismic faulting and the upper transition from stable to unstable slip regimes. Geophys. Res. Lett., 15: 621–624.

Matsuda, T., 1977. Estimation of future destructive earthquakes from active faults on land in Japan. J. Phys. Earth, 25 (Suppl.), pp. S251–S260.

Matsu'ura, M., Kataoka, H. and Shibazaki, B., 1992. Slip-dependent friction law and nucleation processes in earthquake rupture. In: T. Mikumo, K. Aki, M. Ohnaka, L.J. Ruff and P.K.P. Spudich (Editors), Earthquake Source Physics and Earthquake Precursors. Tectonophysics, 211: 135–148.

Matsu'ura, S.R., Karakama, I. and Tsumura, K., 1988. List of Earthquakes in the Kanto Area and Its Vicinity. Earthquake Res. Inst., Univ. Tokyo.

Meredith, P.G. and Atkinson, B.K., 1985. Fracture toughness and subcritical crack growth during high-temperature tensile deformation of Westerly granite and Black gabbro. Phys. Earth Planet. Inter., 39: 33–51.

Ohnaka, M., 1990. Nonuniformity of crack-growth resistance and breakdown zone near the propagating tip of a shear crack in brittle rock: a model for earthquake nucleation to dynamic rupture. Can. J. Phys., 68: 1071–1083.

Ohnaka, M. and Kuwahara, Y., 1990. Characteristic features of local breakdown near a crack-tip in the transition zone from nucleation to unstable rupture during stick-slip shear failure. Tectonophysics, 175: 197–220.

Ohnaka, M. and Yamamoto, K., 1984. Experimental studies of failure nucleation and propagation along simulated faults in rock. In: R. Sato (Editor), Study on Short-Period Behavior in Fault Motion and Estimation of Input Seismic Motion. Final Tech. Rep. A-59-3, Univ. Tokyo, Tokyo, pp. 11–46.

Ohnaka, M. and Yamashita, T., 1989. A cohesive zone model for dynamic shear faulting based on experimentally inferred constitutive relation and strong motion source parameters. J. Geophys. Res., 94: 4089–4104.

Ohnaka, M., Kuwahara, Y., Yamamoto, K. and Hirasawa, T., 1986. Dynamic breakdown processes and the generating mechanism for high-frequency elastic radiation during stick-slip instabilities. In: S. Das, J. Boatwright and C.H. Scholz (Editors), Earthquake Source Mechanics. Am. Geophys. Union, M. Ewing Vol. 6, Geophys. Monogr., 37: 13–24.

Ohnaka, M., Kuwahara, Y. and Yamamoto, K., 1987. Constitutive relations between dynamic physical parameters near a tip of the propagating slip zone during stick-slip shear failure. Tectonophysics, 144: 109–125.

Okubo, P.G. and Aki, K., 1987. Fractal geometry in the San Andreas fault system. J. Geophys. Res., 92: 345–355.

Paterson, M.S., 1978. Experimental Rock Deformation—The Brittle Field. Springer, Berlin, 254 pp.

Power, W. and Tullis, T.E., 1991. Euclidean and fractal models for the description of rock surface roughness. J. Geophys. Res., 96: 415–424.

Power, W.L., Tullis, T. and Weeks, J.D., 1988. Roughness and wear during brittle faulting. J. Geophys. Res., 93: 15268–15278.

Rice, J.R. and Ruina, A.L., 1983. Stability of steady frictional slipping. J. Appl. Mech., 50: 343–349.

Ruina, A.L., 1983. Slip instability and state variable friction laws. J. Geophys. Res., 88: 10359–10370.

Savage, J.C. and Burford, R.O., 1973. Geodetic determination of relative plate motion in central California. J. Geophys. Res., 78: 832–845.

Scholz, C.H., 1988a. Mechanisms of seismic quiescences. Pure Appl. Geophys., 126: 701–718.

Scholz, C.H., 1988b. The brittle–plastic transition and the depth of seismic faulting. Geol. Rundsch., 77: 319–328.

Scholz, C.H., 1988c. The critical slip distance for seismic faulting. Nature, 336: 761–763.

Scholz, C.H. and Aviles, C.A., 1986. The fractal geometry of faults and faulting. In: S. Das, J. Boatwright and C.H. Scholz (Editors), Earthquake Source Mechanics. Am. Geophys. Union, M. Ewing Vol. 6, Geophys. Monogr., 37: 147–155.

Shimazaki, K. and Somerville, P., 1979. Static and dynamic parameters of the Izu–Oshima, Japan earthquake of January 14, 1978. Bull. Seismol. Soc. Am., 69: 1343–1378.

Sibson, R.H., 1982. Fault zone models, heat flow, and the depth distribution of earthquakes in the continental crust of the United States. Bull. Seismol. Soc. Am., 72: 151–163.

Sibson, R.H., 1984. Roughness at the base of the seismogenic zone: contributing factors. J. Geophys. Res., 89: 5791–5799.

Stesky, R.M., 1975. The Mechanical Behavior of Faulted Rock at High Temperature and Pressure. Ph.D. thesis, MIT, Cambridge.

Stesky, R.M., 1978. Mechanisms of high temperature frictional sliding in Westerly granite. Can. J. Earth Sci., 15: 361–375.

Stesky, R.M., Brace, W.F., Riley, D.K. and Bobin, P.-Y.F., 1974. Friction in faulted rock at high temperature and pressure. Tectonophysics, 23: 177–203.

Tse, S.T. and Rice, J.R., 1986. Crustal earthquake instability in relation to the depth variation of frictional slip properties. J. Geophys. Res., 91: 9452–9472.

Tsumura, K., Karakama, I., Ogino, I. and Takahashi, M., 1978. Seismic activities before and after the Izu–Oshima-kinkai earthquake of 1978. Bull. Earthquake Res. Inst., Univ. Tokyo, 53: 675–706.

Tullis, J. and Yund, R.A., 1977. Experimental deformation of dry Westerly granite. J. Geophys. Res., 82: 5705–5718.

Tullis, J. and Yund, R.A., 1980. Hydrolytic weakening of experimentally deformed Westerly granite and Hale albite rock. J. Struct. Geol., 2: 439–451.

Turcotte, D.L. and Spence, D.A., 1974. An analysis of strain accumulation on a strike slip fault. J. Geophys. Res., 79: 4407–4412.

U.S. Geological Survey Staff, 1990. The Loma Prieta, California, earthquake: an anticipated event. Science, 247: 286–293.

Wawersik, W.R. and Brace, W.F., 1971. Post-failure behavior of a granite and diabase. Rock Mech., 3: 61–85.

Wong, T.-F., 1982a. Effects of temperature and pressure on failure and post-failure behavior of Westerly granite. Mech. Mater., 1: 3–17.

Wong, T.-F., 1982b. Shear fracture energy of Westerly granite from post-failure behavior. J. Geophys. Res., 87: 990–1000.

Yamashita, T. and Ohnaka, M., 1991. Nucleation process of unstable rupture in the brittle regime: a theoretical approach based on experimentally inferred relations. J. Geophys. Res., 96: 8351–8367.

Yamashita, T. and Ohnaka, M., 1992. Precursory surface deformation expected from a strike-slip fault model into which rheological properties of the lithosphere are incorporated. In: T. Mikumo, K. Aki, M. Ohnaka, L.J. Ruff and P.K.P. Spudich (Editors), Earthquake Source Physics and Earthquake Precursors. Tectonophysics, 211: 179–199.